# 3D Modelling and Finite Element Analysis of Ankle Joint Using Computed Tomography (CT) Data

**A Thesis Submitted**
**In Partial Fulfillment of the Requirements for theDegree**
**of**

## MASTER OF TECHNOLOGY

**in**
**Computational Design**
**By**


**PRAVAS**
**(2K13/CDN/10)**


**Under the Supervision of**
**R.C. Singh and Ranganath M.S.,**
**Assistant Professor, Department of Mechanical Engineering,**
**Delhi Technological University**



**Department of Mechanical Engineering**

**DELHI TECHNOLOGICAL UNIVERSITY**
**(Formerly Delhi College of Engineering)**
**Shahbad Daulatpur, Main Bawana Road, Delhi-110042, India**


**August, 2015**

# Declaration

I Pravas, student of M. Tech. (Computational Design) under roll no. 2K13/CDN/10 of Department of Mechanical Engineering, Delhi Technological University, Bawana Road, Delhi declare that Major-II project report on "3D Modelling and Finite Element Analysis of Ankle Joint Using Computed Tomography (CT) Data" submitted in partial fulfilment of award of Degree of Masters of Technology under specialization in Computational Design is the original work conducted by me.

The information and data given in the report is authentic to the best of my knowledge. This report is not being submitted to any other university for award of any other Degree, Diploma or Fellowship.

Pravas

Date: (2K13/CDN/10)

# Certificate

This is to certify that the Major-II Project Report entitled “3D Modelling and Finite Element Analysis of Ankle Joint Using Computed Tomography (CT) Data” is a bonafide work carried out by Mr. Pravas (2K13/CDN/10) and submitted to Department of Mechanical Engineering, Delhi Technological University, Delhi in the partial fulfilment of the requirement for the award of the Degree of the Masters of Technology under specialization in Computational Design under our supervision. It is further certified that the embodied work has not been submitted to any other institution for the award of other degree or certificate.


R. C. Singh
Assistant Professor
Department of Mechanical Engg.
Delhi Technological University

Ranganath M.S.
Assistant Professor
Department of Mechanical Engg.
Delhi Technological University

# Acknowledgements

Firstly, I would like to express my sincerest gratitude to my guides, Dr. R.C. Singh (Asst. Professor, Department of Mechanical Engineering) and Dr. Ranganath M.S. (Asst. Professor, Department of Mechanical Engineering) for constant support and valuable guidance throughout the duration of this project.

I would also like to thank Dr. R. S. Mishra (Head of the Department, Department of Mechanical Engineering) for his constant encouragement and support to the students. I also wish to thank the other faculty members and technical staff of DTU without whose help and support this project could not have been completed.

Finally, I extend my thanks to all my friends and family members for their love, support, patience, forgiveness, and inspiration.

Date:

Pravas

2K13/CDN/10

# Abstract

The ankle joint (or talocrural joint) is a synovial joint located in the lower limb. It is formed by the bones of the leg and the foot – the tibia, fibula and talus. Functionally, it is a **hinge type** joint, permitting dorsiflexion and plantarflexion of the foot. In this research, theanalysis of total deformation and Von Mises Stress on the ankle joint was carried out for various loads applied on it with different boundary conditions. The objective of this study is the detailed study of ankle joint and to develop a 3D solid model of ankle joint and analyse with a consistent set of forces of body weight to validate this developed model under static loading conditions.

Computed Tomography (CT) scan images are used to obtain the geometry of interest. Image processing & computer-aided design (CAD) software tools are employed to obtain the 3D solid model of the tibia, fibula and talus from CT images. Finite Element Analysis (FEA) of robust 3D solid model of tibia, fibula and talus is done through ANSYS. Results of this study are helpful for the orthopaedic surgeon to understand the mechanical behaviour of the ankle joint and in prosthesis of human leg and foot and implant designing & fixation and can develop a better implant on the basis of these results.

# Table of Contents

# List of Figures

# List of Tables

# CHAPTER 1

# INTRODUCTION

## 1.1 Biomechanics

Biomechanics is the study of application of engineering principles and ways to biology so as to perceive the mechanics of the living systems, significantly their movement and structure. It'sclosely complex with medical physics, physiology, anatomy and biomaterials thus it may be thought of as a sub-branch of medicine engineering (or bio engineering). Medicine Engineering is associate degree engineering field which mixes the ideas of engineering principles and style with drugs and biology for health care functions, as well as designation, observance and medical aid.

Biomechanics isn't a replacement field; it came into existence in 1899. Early efforts during this field were created by philosopher, Galileo Galilei and Leonhard Euler. Throughout the last twenty years, development in biomechanics increased attributable to 2 reasons: 1st, the event of computers and process ways in engineering mechanics that realistically describe and with success analyse advanced mechanical behaviour of biological tissue; and second, the increasing stress on surgical reconstruction of the body components for disabled and sick.

Biomechanics has participated nearly in every modern advanced technology of medical sciences. It's many fields of application like orthopaedic & vessel surgery, medicine, rehabilitation, dentistry and sports. Thus, it's closely associated with identification, surgery and prosthesis. Long run success of these surgeries and restorative desires style

and surgical techniques that support a sound understanding of human musculoskeletal mechanics.

## 1.2 Ankle Joint

### 1.2.1 Overview

The ankle joint is a hinged synovial joint with primarily up-and-down movement (plantarflexion and dorsiflexion). However, once the range of motion of the ankle joint and subtalar joints (talocalcaneal and talocalcaneonavicular) is taken along, the sophisticated functions as a universal joint (see the image below).

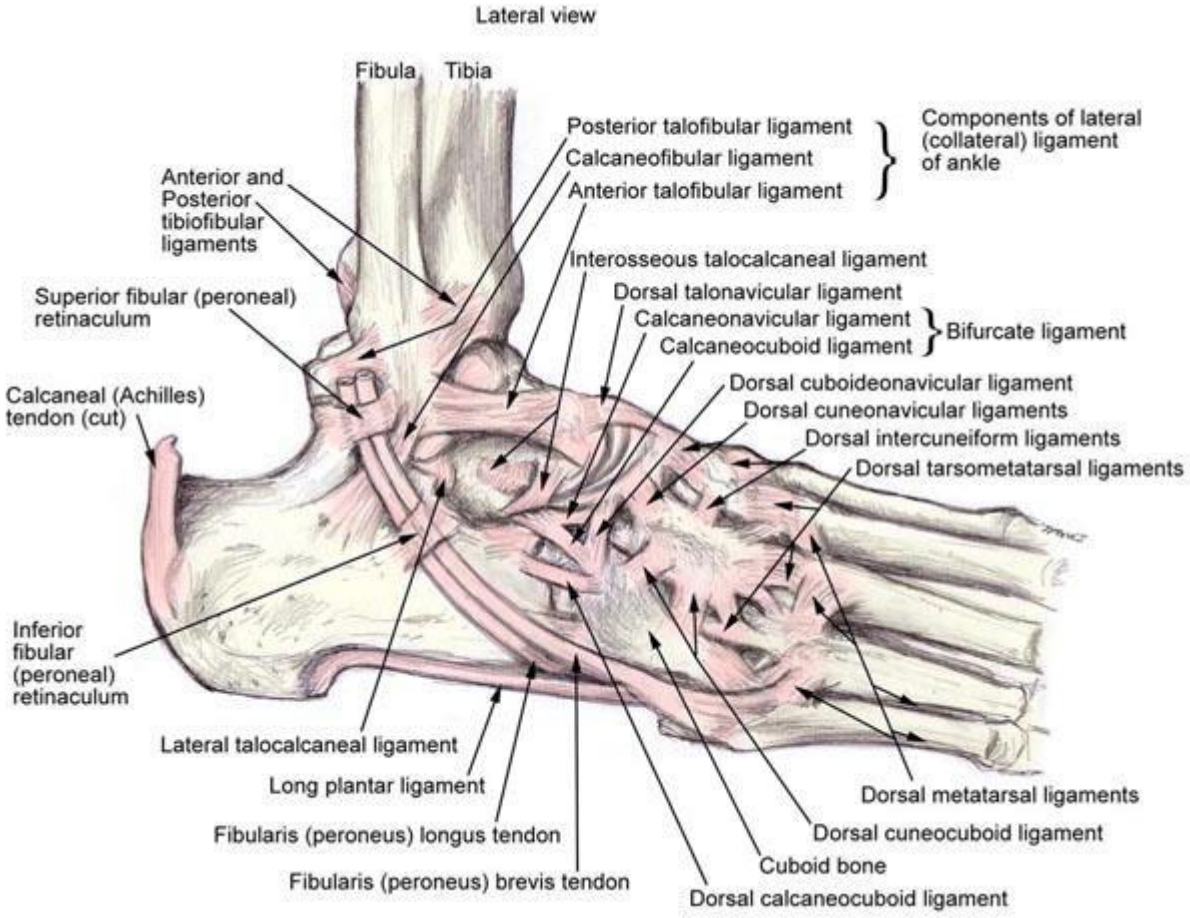


Figure 1Anatomy of the lateral ankle ligamentous complex and related structures.

The combined movement among the dorsiflexion and plantarflexion directions is larger than 100°; bone-on-bone abutment on the way side this range protects the anterior and posterior ankle capsular ligaments from injury. The anterior and posterior ankle capsular ligaments are relatively thin compared with the medial and lateral ankle ligaments.

Type I collagen tissue constitutes the bulk of the capsule and supporting ligaments of the ankle. The fibre density and orientation are organized dynamically per the quality mechanical stress experienced by the joint. inside limits, the larger the excursion of the joint capsule and ligaments, the less apparently sprains are to occur. With exaggerated motion, the muscles absorb the mechanical force energy without surpassing the tensile limits of either the joint capsule or the ligaments.

### 1.2.2 Lateral Ligament Anatomy and Biomechanics

The lateral complex of ligaments has 3 elements (see in the image below):

- Anterior talofibular ligament (ATFL)
- Calcaneofibular ligament (CFL)
- Posterior talofibular ligament (PTFL)

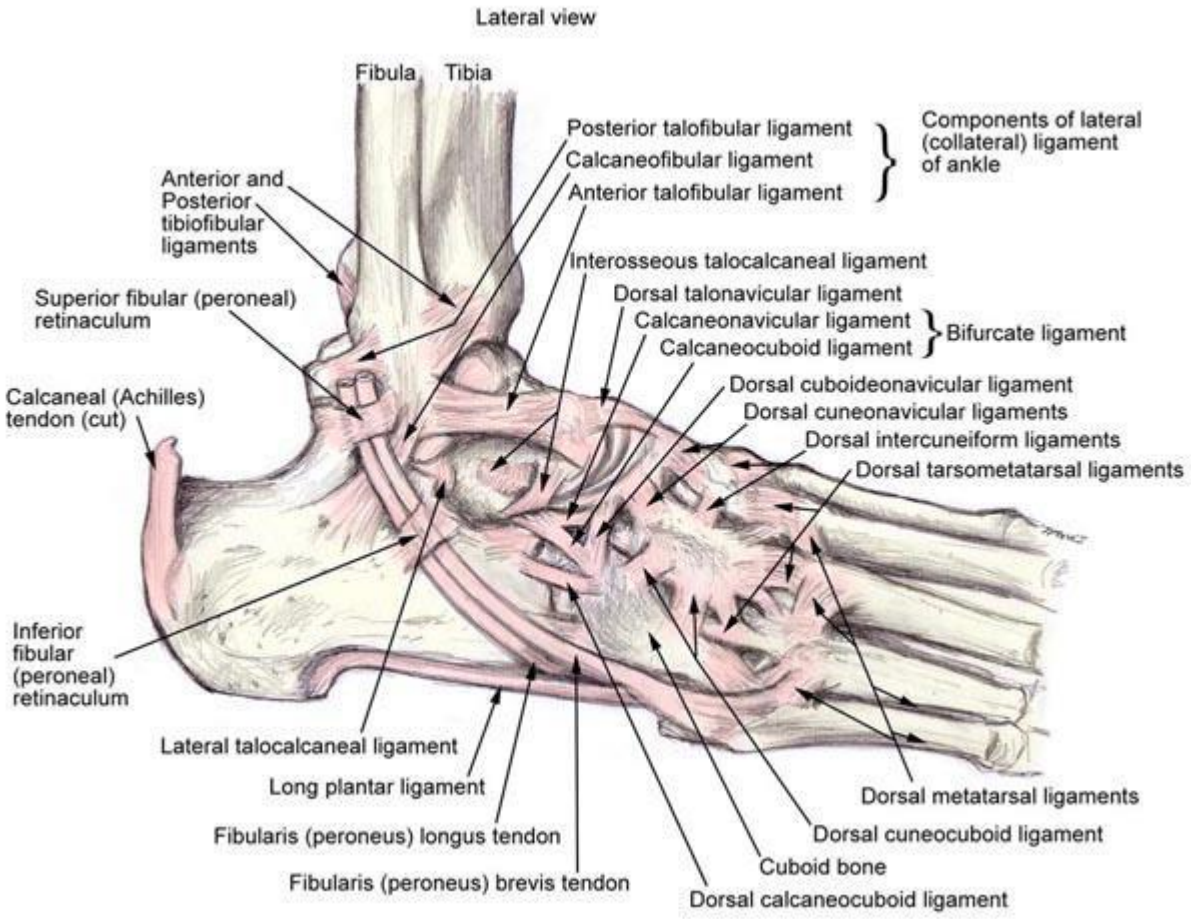


The subtalar joint is known differently by different groups. The anatomic subtalar (talocalcaneal) joint refers structurally to the articulation between the talus and also the underlying calcaneus. Orthopedicians, however, consider the functional subtalar joint consisting of the anatomic subtalar joint and the talocalcaneal a part of the talocalcaneonavicular joint; it's impossible for the 2 joints to perform severally.

In the anatomic subtalar (talocalcaneal) joint, the lateral complex consists of the subsequent four ligaments:

- CFL (note that the CFL spans the tibiotalar and talocalcaneal joints)
- Lateral talocalcaneal ligament (LTCL)
- Cervical ligament (CL)

• Interosseous talocalcaneal ligament (IOL; this ligament provides an axis of rotation concerning movement happens in the talocalcaneal joint)

## Biomechanical function

In addition to the standard anatomy of the ankle joint, note the biomechanical function of every part in stabilising the joint. The ATFL is loose, and the CFL is taut in dorsiflexion. However, the ATFL is taut and the CFL is loose in plantarflexion. The PTFL is stressed to maximum in dorsiflexion.

The CFL is cordlike and thicker and stronger than the ATFL, it runs from the tip of the lateral malleolus to the lateral side of the calcaneus bones directly below the fibula. The CFL prevents motion and acts virtually independently in neutral and in dorsiflexed positions.

The ATFL contains a lower load to failure than the CFL; i.e., the maximum capacity load to failure of the CFL is roughly 2-3.5 times larger than that for the ATFL. [1] But, in distinction to the CFL and PTFL, the ATFL can bear the largest quantity of deformation (strain) before failure and permits for internal rotation of the talus throughout plantarflexion. Within the mortise the ATFL restricts internal rotation of the talus primarily; while in plantarflexion, the ATFL inhibits movement.

The PTFL is the strongest of the 3 parts of the lateral ankle joint. It runs nearly horizontally from the fossa within the inner side of the tip of the lateral malleolus to the posterior tubercle of the talus. In dorsiflexion, the PTFL inhibits external rotation with the ankle joint. Note that medial ligaments are the first restrictors of dorsiflexion (see the image below) which the PTFL solely assists during this function. The short fibers of the PTFL may also limit internal rotation after rupture of the ATFL. The PTFL inhibits motion with the

ankle joint in dorsiflexion after disruption of the CFL.

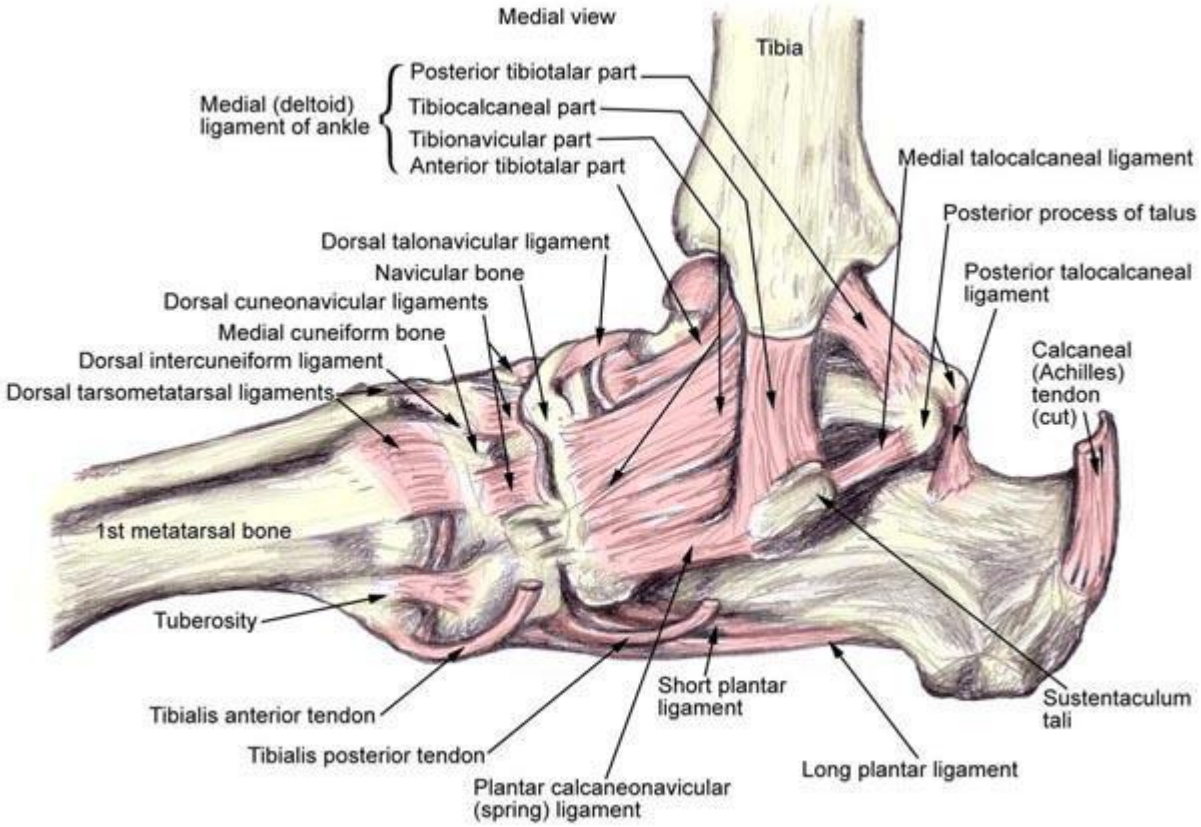


Figure 2Medial ankle view showing the ligamentous anatomy of the deltoid ligament and related structures.

### 1.2.3Medial Ligament Anatomy and Biomechanics

The deltoid ligament is part into the consequent 2 sections (see the picture underneath):

- Superficial deltoid ligament
- Deep deltoid ligament

The shallow deltoid ligament begins from a front hard noticeable quality of the average malleolus referred to clinically as the foremost colliculus. The tibionavicular bit embeds onto the navicular and is the most front part; the tibiocalcaneal segment starts at the

foremost colliculus and inserts onto the sustentaculumtali; and the last piece of the shallow deltoid is the posterior tibiotalar ligament (PTTL).

The profound deltoid ligament begins from the intercollicular depression and posterior bony prominence known clinically as the back colliculus. It's shorter and thicker than the superficial poertion and is touching with the average case of the lower leg joint and the average part of the interosseous talocalcaneal ligament (IOL).

The best mechanical forces over the ankle joint are coordinated medially in the traditional external rotation of the foot in strolling and running. This is reflected in the quality and thickness of the deltoid ligament.

### Biomechanical function

Biomechanically, the deltoid ligament fundamentally counteracts snatching. After division of both parts of the deltoid ligament, anterior instability of the ankle does not increase. Once the sidelong ligaments are cut, the deltoid ligament goes about as an optional limitation against anterior translation. The fibular ligament basically restrains sidelong interpretation of the bone. The profound deltoid ligament gives the best limitation against horizontal interpretation. So as to tilt the bone in valgus inside of the mortise, the shallow and profound deltoid ligaments must be completely ruptured.

### 1.2.4Syndesmosis and Biomechanics

The syndesmosis of the ankle refers to the membrane connecting the tibia to the fibula. The tibia and fibula are connected throughout their length by an interosseous membrane. However, there are 3 determinable ligaments at the ankle, as follows:

- Anterior (anteroinferior) tibiofibular (AITF) ligament - this is the most ordinarily injured ligament in syndesmotic sprains

- Posterior (posteroinferior) tibiofibular (PITF) ligament - This ligament contains a deep portion, known as the transverse tibiofibular ligament, and a superficial portion

- Interosseous tibiofibular ligament - This ligament is found between the nearly congruent distal surfaces of the tibia and fibula and is the primary bond holding the bones together; superiorly, the interosseous tibiofibular ligament is contiguous with the interosseous membrane, that provides some further strength to the syndesmosis

## Biomechanical function

Biomechanically, with respect to the distal ends of the tibia and fibula a certain amount of motion is allowed in all planes. The distance between the lateral and medial malleoli increases by approximately 1.5 mm when the ankle goes from full plantarflexion to full dorsiflexion. Rotation of the tibia on the talus can also occur while a person is walking. This rotation can be as much as 6°.

The AITF ligament provides approximately 35% of ankle stability; the deep PITF, 33%; the interosseous PITF, 22%; and the superficial PITF, 9%.[2] Ogilvie-Harris et al experimentally demonstrated the importance of the syndesmotic ligaments to ankle stability by sectioning the ligaments.[2] Rasmussen demonstrated that the ligaments of the syndesmosis play little role in the stability of the ankle as long as the other ligamentous structures are intact.[3] No study exists in which a purely ligamentous injury to the syndesmosis has been produced through externally applied stress (ie, external rotation and abduction).

### 1.2.5Subtalar Joint and Ligament Anatomy and Biomechanics

The subtalar joint (talocalcaneal joint) can be divided into anterior and posterior articulations that are separated by the sinus tarsi and the tarsal canal . The anterior portion of the talus, the posterior surface of the navicular, the anterior part of the calcaneus, and the calcaneonavicular ligament and the fibrous capsule form the anterior subtalar joint (talonavicular). The posterior facet of the inferior surface of the talus and the corresponding posterior facet of the calcaneus form the posterior talocalcaneal portion.

The calcaneofibular ligament (CFL), lateral talocalcaneal ligament (LTCL), cervical ligament (CL), and the interosseous talocalcaneal ligament (IOL)are the primary ligaments of the subtalar joint (talocalcaneal joint). The CL is believed to be the strongest bond between the talus and the calcaneus.

Harper categorized the ligamentous structures of the subtalar joint (talocalcaneal joint) in layers, as follows[4] :

- The superficial layer consists of the lateral root of the LTCL and CFL
- The intermediate layer consists of the CL
- The deep layer contains the medial IOL

#### Biomechanical function

The motion of the subtalar joint (talocalcaneal joint) is flexion-supination-adduction or extension-pronation-abductionfrom a biomechanical standpoint. The motion occurs via talar ovoid surfaces moving over calcaneal ovoid surfaces.

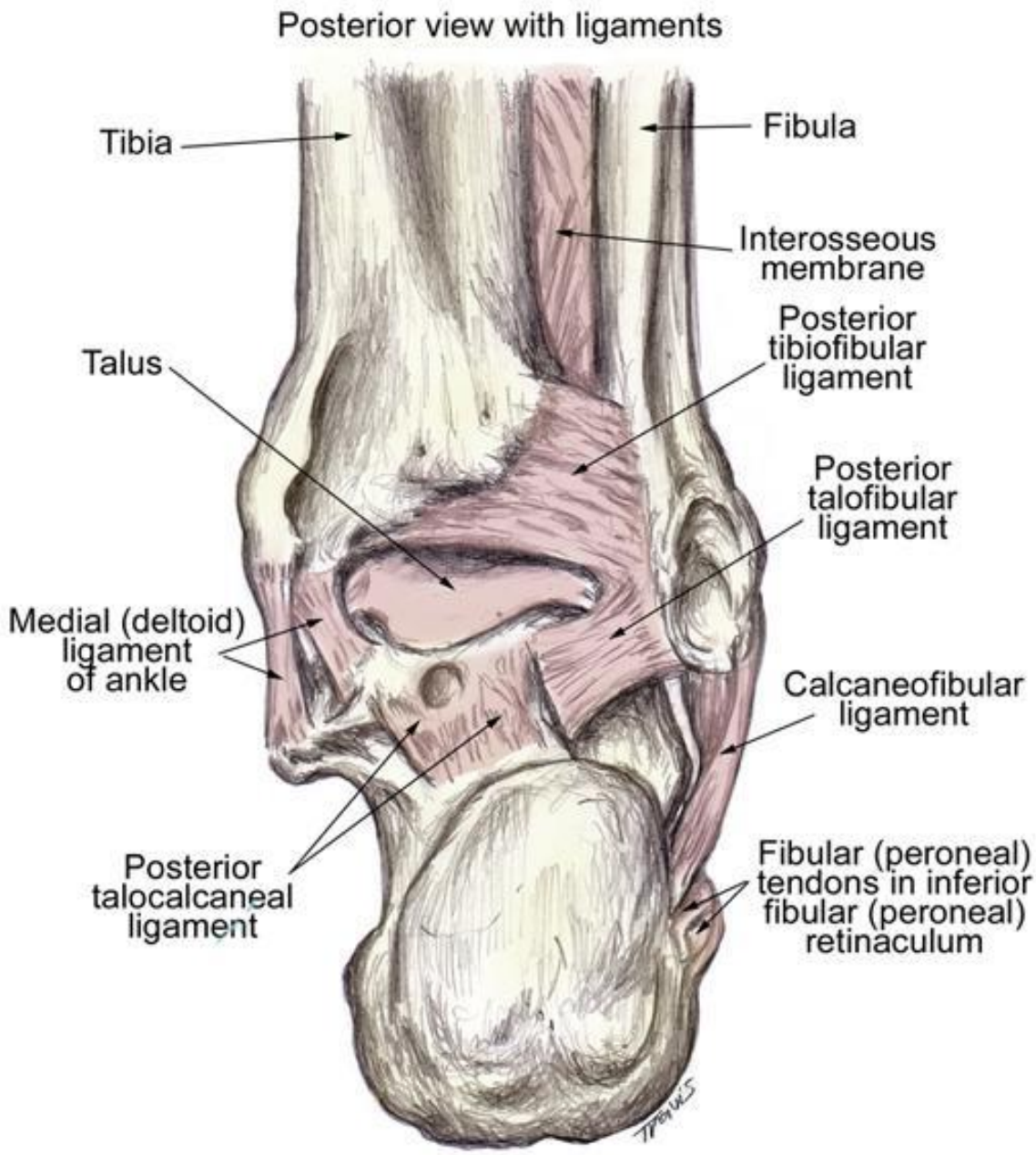


Figure 3 Posterior view of the ligaments of the ankle.

Sectioning studies by Kjaersgaard-Andersen et al showed that sectioning the CL resulted in a 10% increase in rotation, and sectioning of the IOL produced a 21% increase in rotation.[5] In earlier studies, the same authors found a 77% increase in adduction at the subtalar joint (talocalcaneal joint) after sectioning the CFL.[6]

These investigators' findings emphasize the importance of the CFL in providing lateral stability to the subtalar joint (talocalcaneal joint). This conclusion is contrary to that of a study by Cass et al that demonstrated no such influence on subtalar motion.[7] The variability of orientation of the CFL explains thediscrepancy among the studies.

### 1.2.6 Pathophysiologic Variants

The previous sections described the natural anatomy and biomechanics of the lateral complex of ligaments, medial ligaments, ankle syndesmosis, and subtalar joint and ligament. However, there are also three primary anatomic variants, as identified by Trouilloud. These variants include the following[8] :

- *Type A (35%)* –

  A lateral talocalcaneal ligament (LTCL) blends with or reinforces the calcaneofibular ligament (CFL)

- *Type B (25%)*–

  A distinct LTCL is present just anterior to the CFL

- *Type C (42%)*–

  The LTCL is absent

When the CFL is injured in a type A or C anatomic variant, increased subtalar motion is expected.

# CHAPTER 4

# PROCESS METHODOLOGY

A common approach to bone modeling for FE analysis was adopted so as to demonstrate the work, i.e., 3D solid model generation and FE analysis of Ankle Joint. A flow chart indicating step by step work and software used to carry out every step is shown in Figure 4.1. [57].

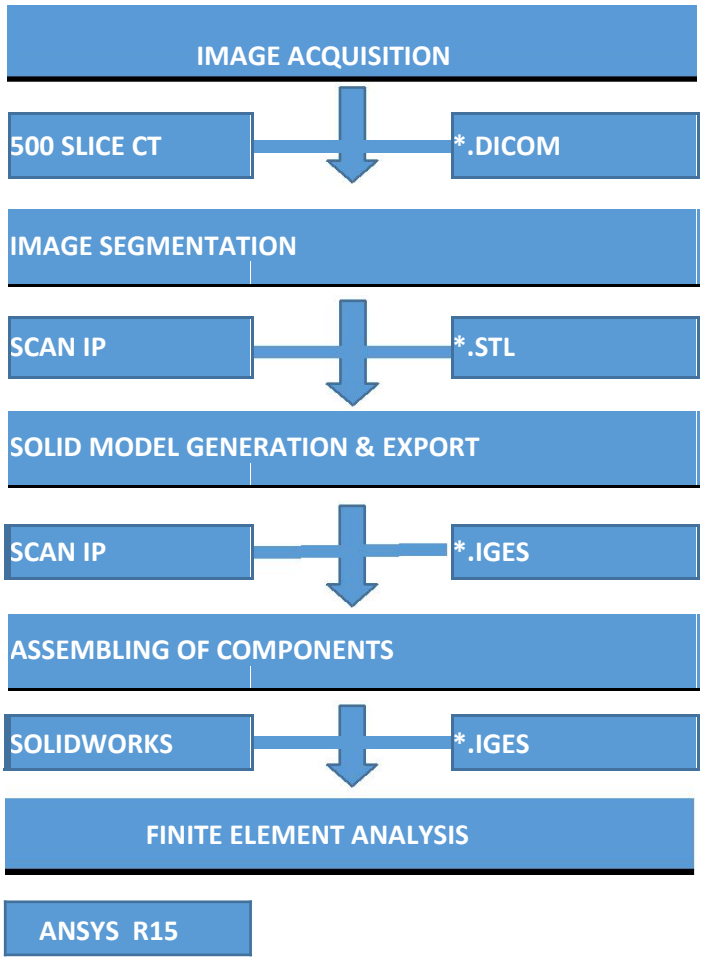


Figure 4.1. Flow chart showing whole research work in steps. The boxes in the left column contain the software tools and the right column boxes indicate the data file extension.

Steps comprising the whole analysis are:

(i) The CT image data that preserves the geometrical information of ankle jointand tibia was acquired.

(ii) A 3D surface model was developed using Trialed license copy of Simpleware Scan IP 6.0, a robust Image visualization & processing software.

(iii) Solidworks 2013 x64 edition, a CAD package, was used for assembling of Ankle Joint and

(iv) For the ultimate step to analyze the mechanical behavior of the developed model, FE analysis was done in ANSYS R14.5.

**4.1. IMAGE DATA ACQUISITION**

In earlier studies, either a frozen (dry) bone, a wet bone, synthetic bone or a bone with apparent density was used for the analysis but in computational biomechanics, particularly for orthopaedic applications, CT has been progressively adopted for bone remodeling since hard tissue contains a high distinction relative to soft tissue (cartilage, muscles, ligaments, etc.) [58], [43]. it is accepted that CT images can offer fairly correct quantitative information on bone geometry which can be connected with the mechanical properties of bone tissues.

CT scan images of lower extremity of a person(age 33 years, female) with healthy tibia, calcaneus, tarsals and metatarsal bones were obtained. The images obtained have vascular phase and were obtained from a 64 slice CT scanner, GE Medical System, apparatus power condition were at 120 KV/350mA. The images acquired were in DICOM (Digital Imaging and Communication in Medicine) format. The folder containing DICOM images were imported to the trial licensed copy of Scan IP 7.0 for further 3D Image visualization, solid model generation, analysis & meshing. The resolution of images was 512x512 with the slice thickness of 0.576172 pixel spacing in both X &Y directions.

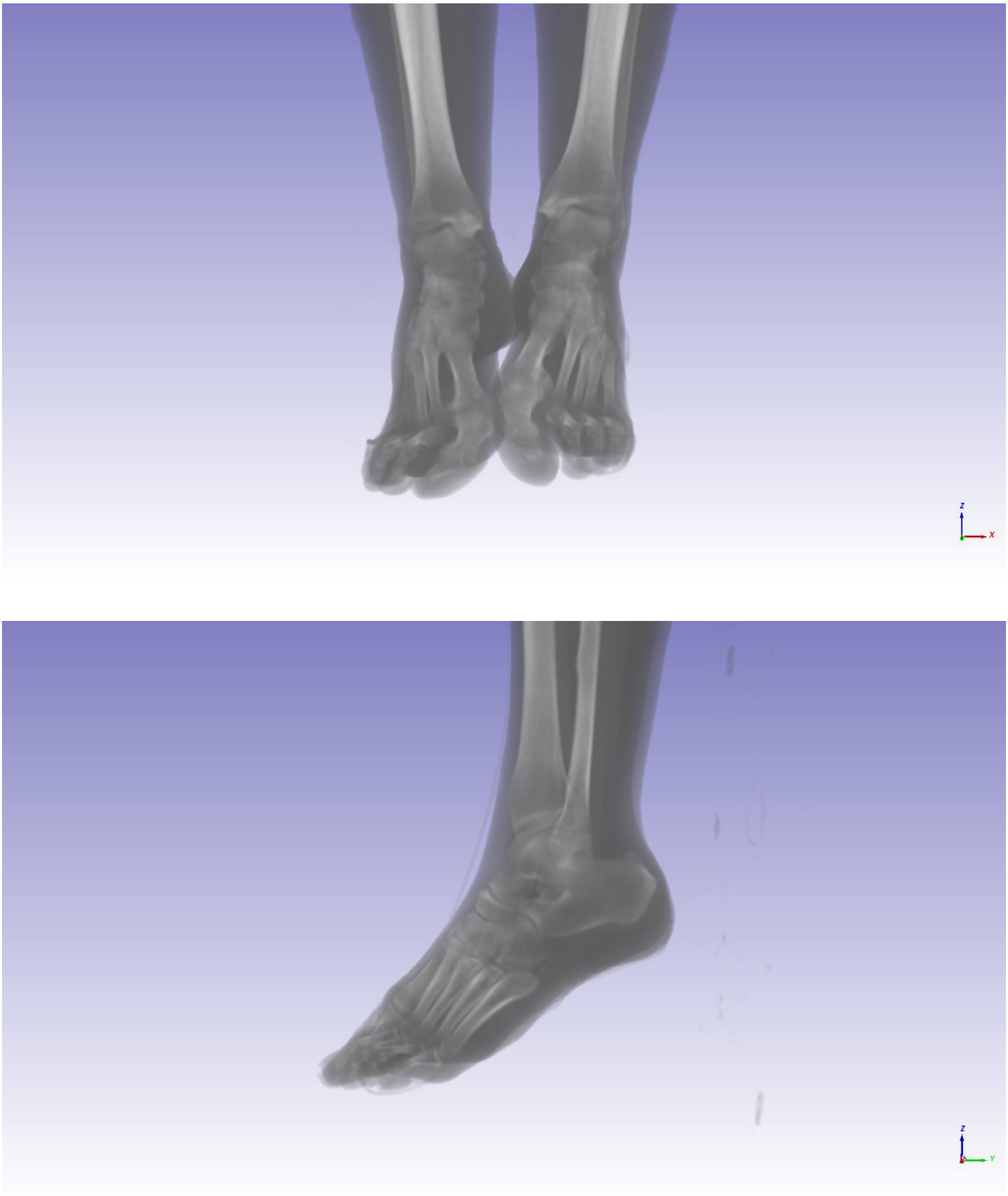


Figure 13 Visualization of the acquired CT image of ankle joint of patient

### 3.2 IMAGE VISUALISATION AND PROCESSING

In presence of image artifacts and signal noise it is necessary to better the resolution and quality of the CT images by proper acquisition parameters as slice thickness and spatial resolution. Also, various digital image processing techniques can be carried out in order to enhance the visual information encompassed in an image.

The loaded image data was then developed for visualization in axial, coronal and sagittal planes. After visualization of the images in the preview, a histogram (Grayscale range -2000 to 2000) was calculated [35] and set to a customized range of window: 427, level: 70 (Figure 13).

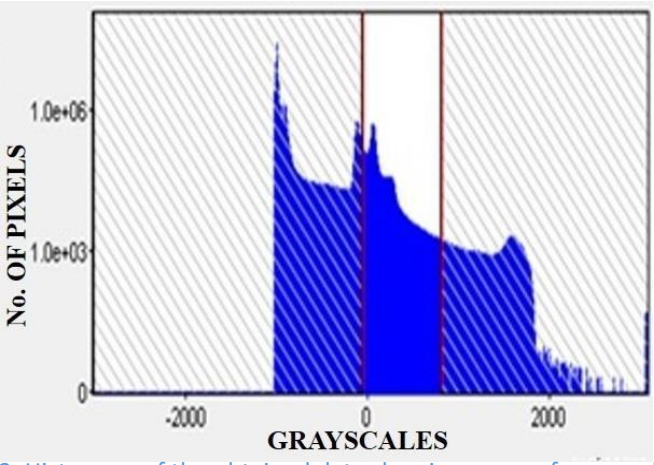


Figure 4.3. Histogram of the obtained data showing range of grey scale.

The next step we move onto is Cropping.Cropping is the simple operation of cutting off parts of the volume in order to only keep data of interest. Sometimes for memory usage purposes, it is recommended to crop your image in order toonly keep the necessary objects within the limits of your volume. Cropping reduces the total no. of slices thereby reducing the computing time as well as reducing the tedious task of segmentation (Figure 15, 16). In this research the no. of slices were reduced from 500 to 126 which in turn reduced the size of the file considerably.

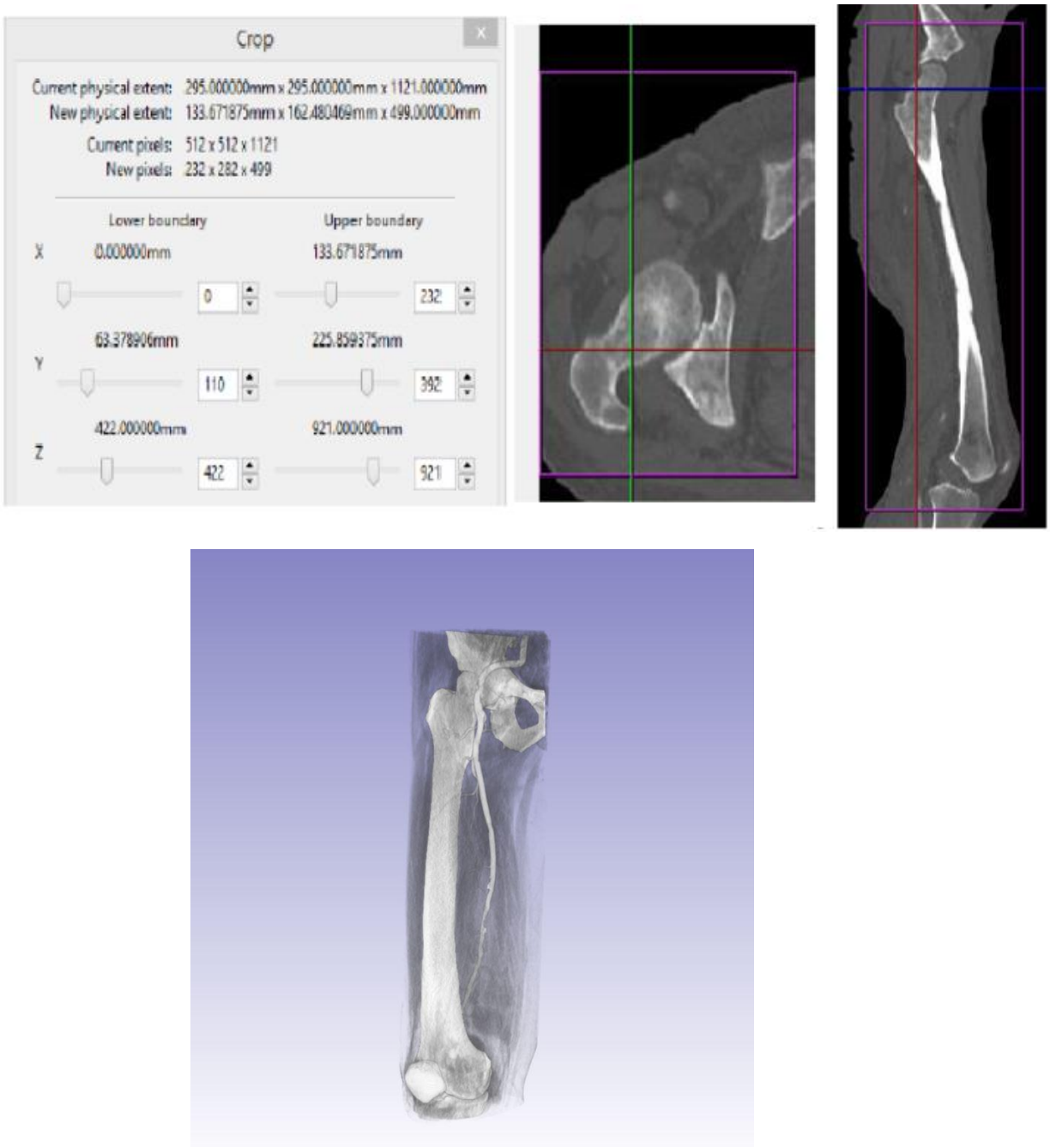


**Figure 15 Snapshot of femur bone being cropped from CT scan image of complete lower extremity**

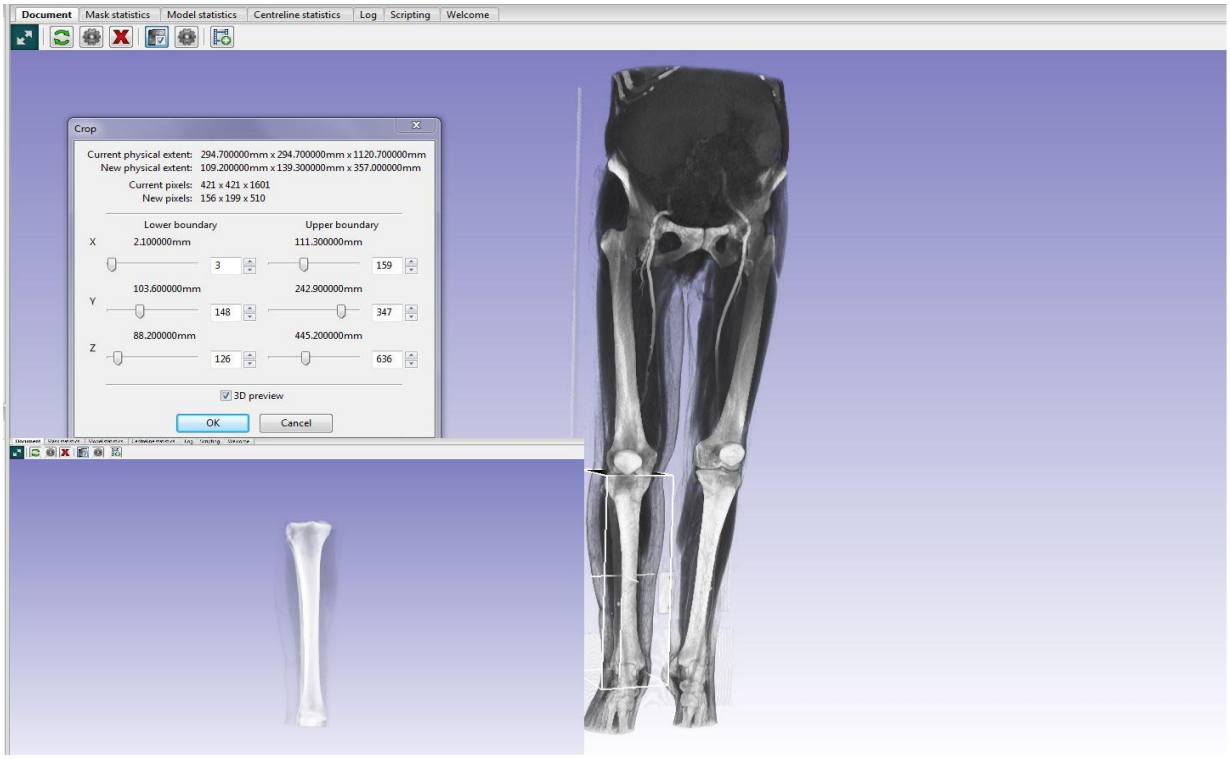


Figure 16 Snapshot of tibia bone being cropped from CT scan image of complete lowerextremity

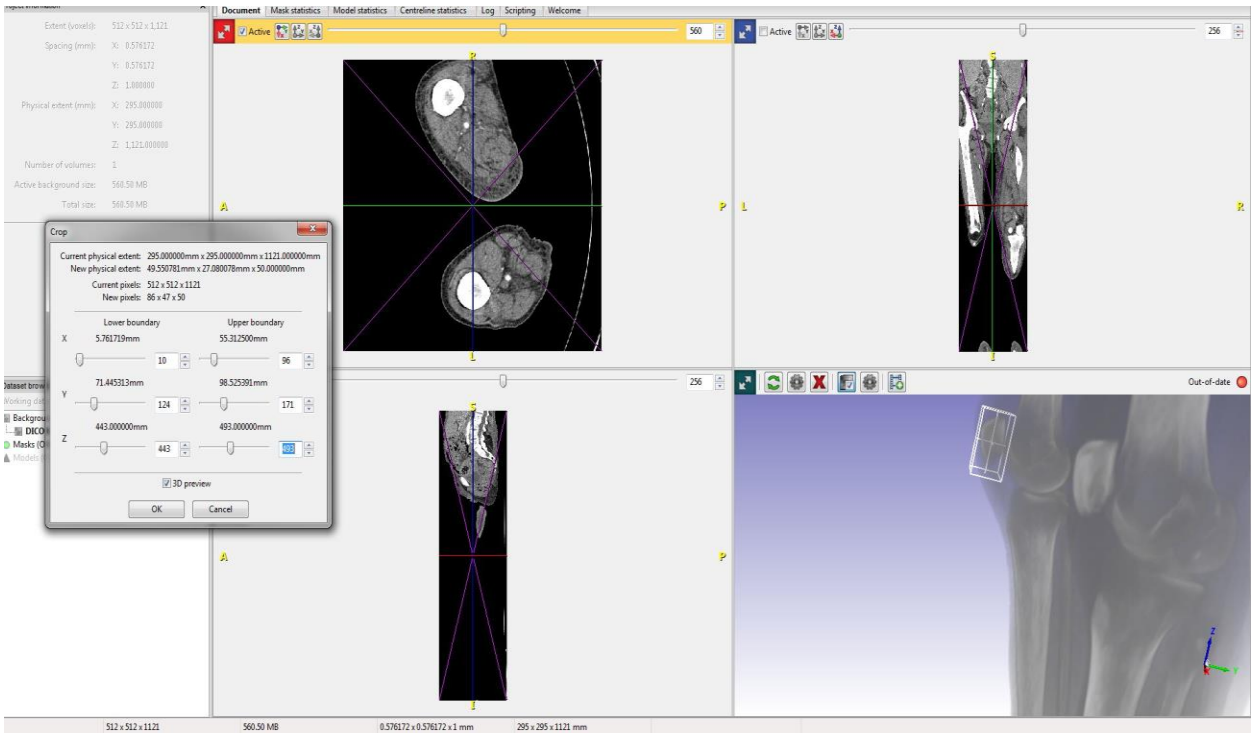


Figure 17 Snapshot of patella being cropped from CT scan image of complete lower extremity

Since, multiple image processing methods are available by which segmentation can be implemented [36]; it solely depends on the requirement as to what traits are to be obtained by the segmentation. Here, segmentation of the femur, tibia& patella bone from the full lower extremity of the CT scan of a person is done.

The subsequent step in modeling is known as image segmentation, that is the segregation of images into non-overlapping areas. In this each area is the locus of an object. It performs an essential role in multiple medical imaging applications by making itsimpler for the delimitation of anatomical constructs and other areas of interest. Generally, this delineation is established on a given image feature like texture or intensity, which is same within a area [37]. Segmentation plays a basic role for anatomical modeling as it forms the conversion between image data and 3-D mesh data. Although, when working with medical images, the segmentation is amongst the extremely difficult tasks to be done within the whole project. It should be considered that a medical image constitues of the data comparitive to the internal parts of the body of human beings, but also of unwanted signals. Objects and blurred ends are some of the features usual to any medical image. Multiple segmentation approaches exist and can be chosen corressponding to the input image. Considering that CT images are the foundation of 3 dimensional medical information for the generation of knee joint constituting the tibia, calcaneuus, tarsals and metatarsal bones. However, segmentation includes a chain of processes, including the ones mentioned above, ScanIP uses the terminology Segmentation for tools that usually use data from the background image to change and/or generate a mask. Segmentation tools can be entirely manual (**Paint**), or supported (**Threshold**, **Paint with threshold**, **Region growing, Flood fill**). Since none of the tools are entirely automated they will need some capability and training in order to provide acceptable results. The phases in the segmentation process are defined for femur below. Similar steps are followed for patella and tibia.

*Threshold* chooses a space of greyscale standard values and is used where segmentation can be attainedon the basis of greyscale intensities. The threshold tool chooses all the voxels in the working background image which has a greyscale value in the designated range. Empowering the interactive Threshold will allow to see the impactwhen sliding the upper and lower value sliders. The standardization instruments can be used to calculate the “right” values to use in the Threshold.Often, the assortment is carried out by simplymaking use of the interactive threshold and selecting an appropriate range by seeing through eye.Greyscale range of 158-1647 is selected.A mask of red colour is used . A Mask is a collecttion of voxels and it overlays the Background image. It is created to choose the areas of interest, then they are added to a Model.

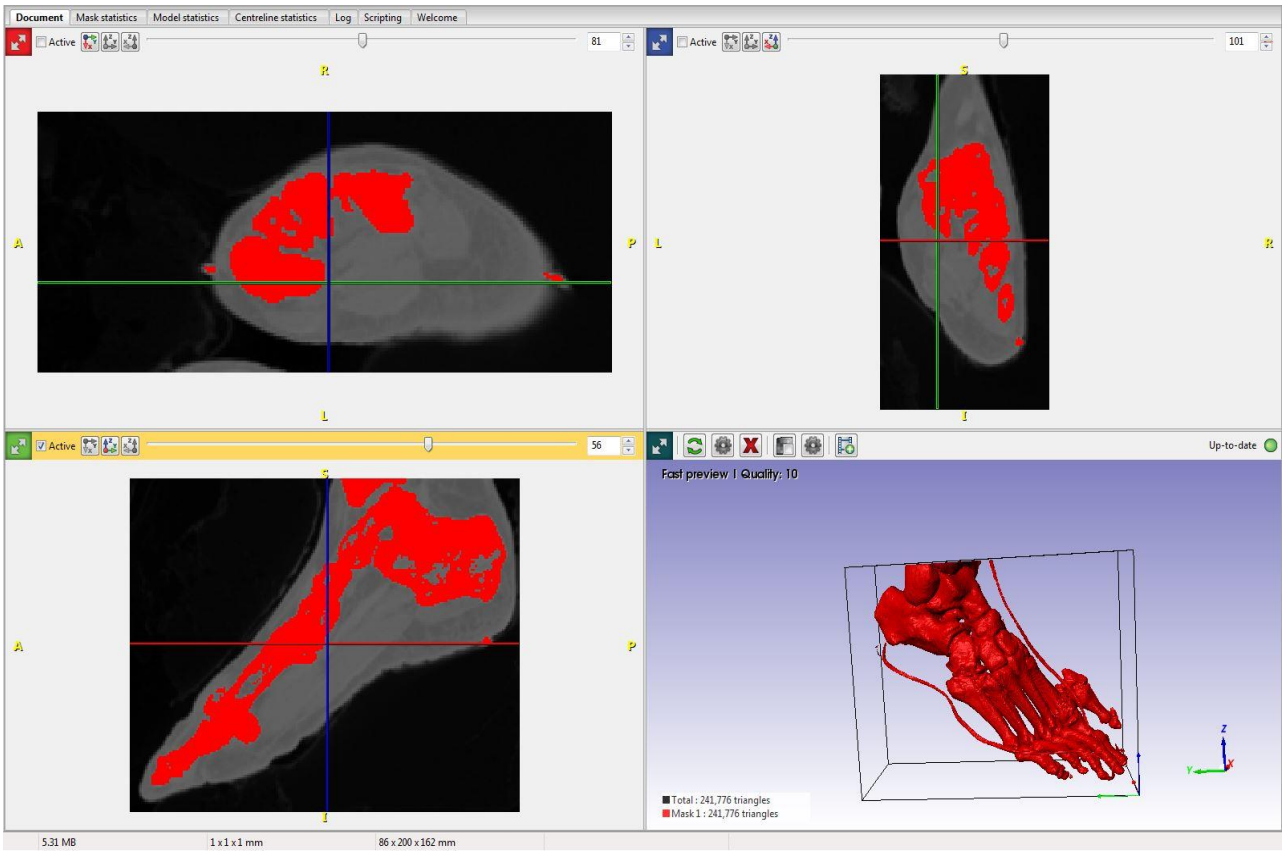


Figure 18 Ankle Foot Model after applying threshold tool

The *Split/Merge tool* is employed to help the end user in slicing masks that should not be connected but have been joined in the segmentation process, or to combine masks that should be connected but were not joined in the early segmentation.

- Split: Slice a mask into multiple masks or areas.
- Merge: Merge multiple masks or areas together.

Markers are employed to direct the Split/Merge tool to the objects that need to be sliced or combined. This is accomplished with the help of a correction mask. When we are executing a Split action, the correction mask must comprise of two/multiple distinctive markers for each object that is required to be sliced. When executing a Merge task, the correction mask must be 1 continuous marker running across the edges of the objects that required to be merged.

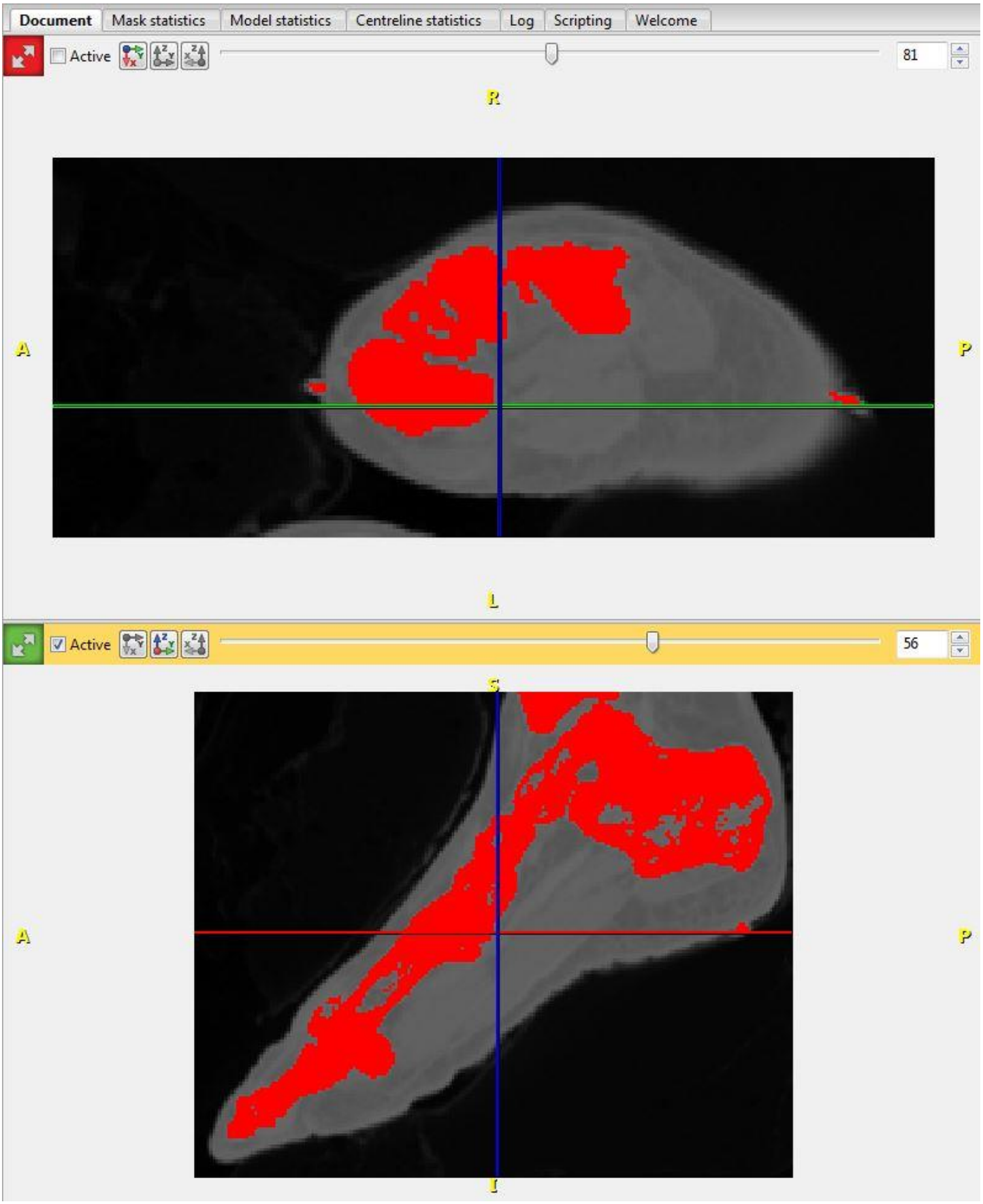


Figure 19 Using split/Merge tool in removal of tibia bone from ankle foot

The segmented foot after the use of split/Merge tool is shown in the following figure:

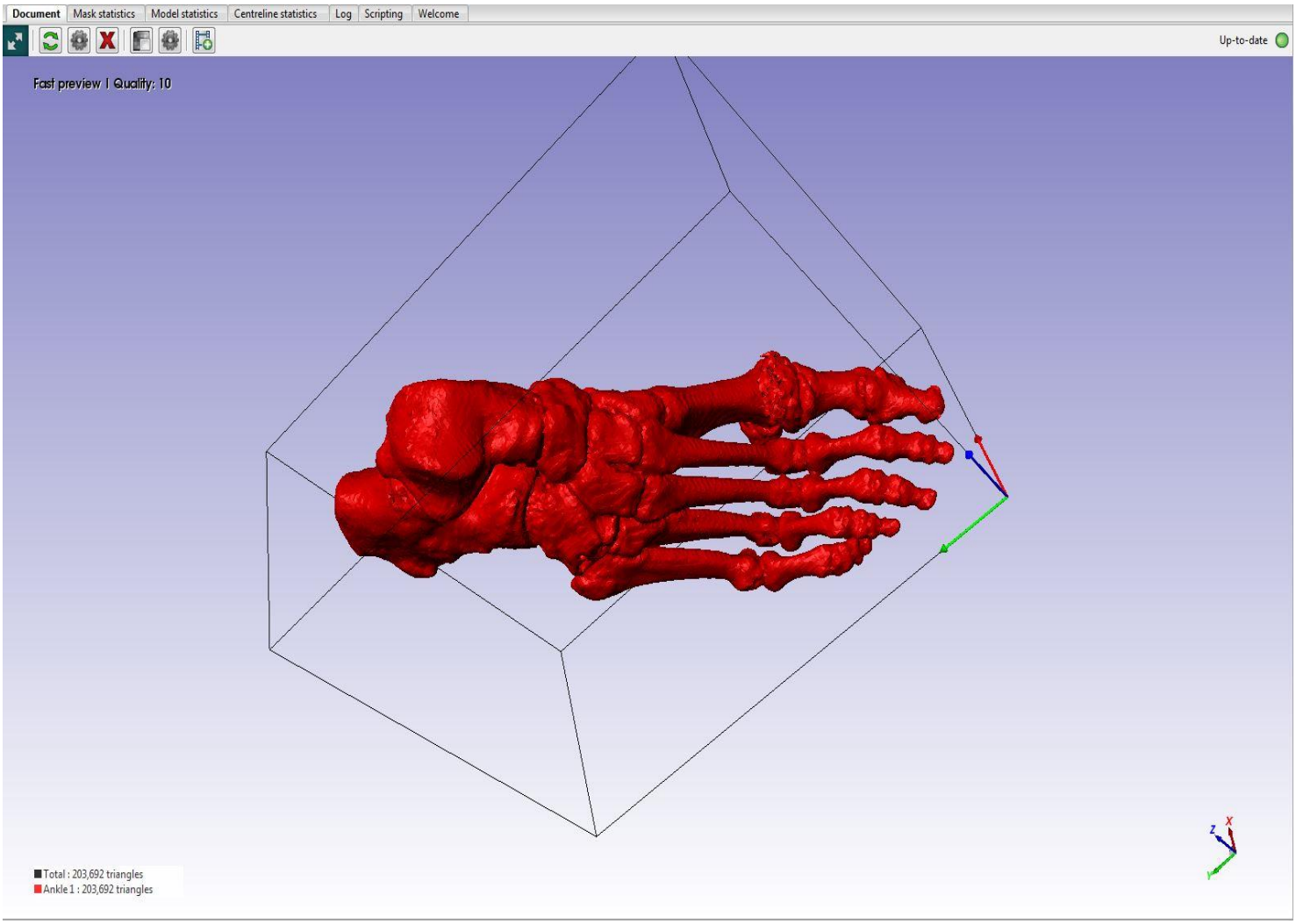


Figure 20 Segmented foot after using split/Merge tool

The next part is the *Smoothning Filter.* Following the completion of the whole segmentation procedure, a sample of the segmented bone iscreated. It is then assesed properly to find any holes/patches in the generated model geometry. Recursive Gaussian filter is used for the smoothing of each mask of the 3D model. It, typically,minimizes image noise and decreases detail levels (Figure 20) [39].

The visual impact of the blurring method is a smooth blur and it is also employed as a pre-processing phase in computer vision algorithm. This is done in order to improve image structures at diverse scales. It is, mathematically, similar to convolving the image using a Gaussian or normal distribution. Since, the Fourier transform of a Gaussian is also a Gaussian, it has the same impact as that of a low pass filtered image.

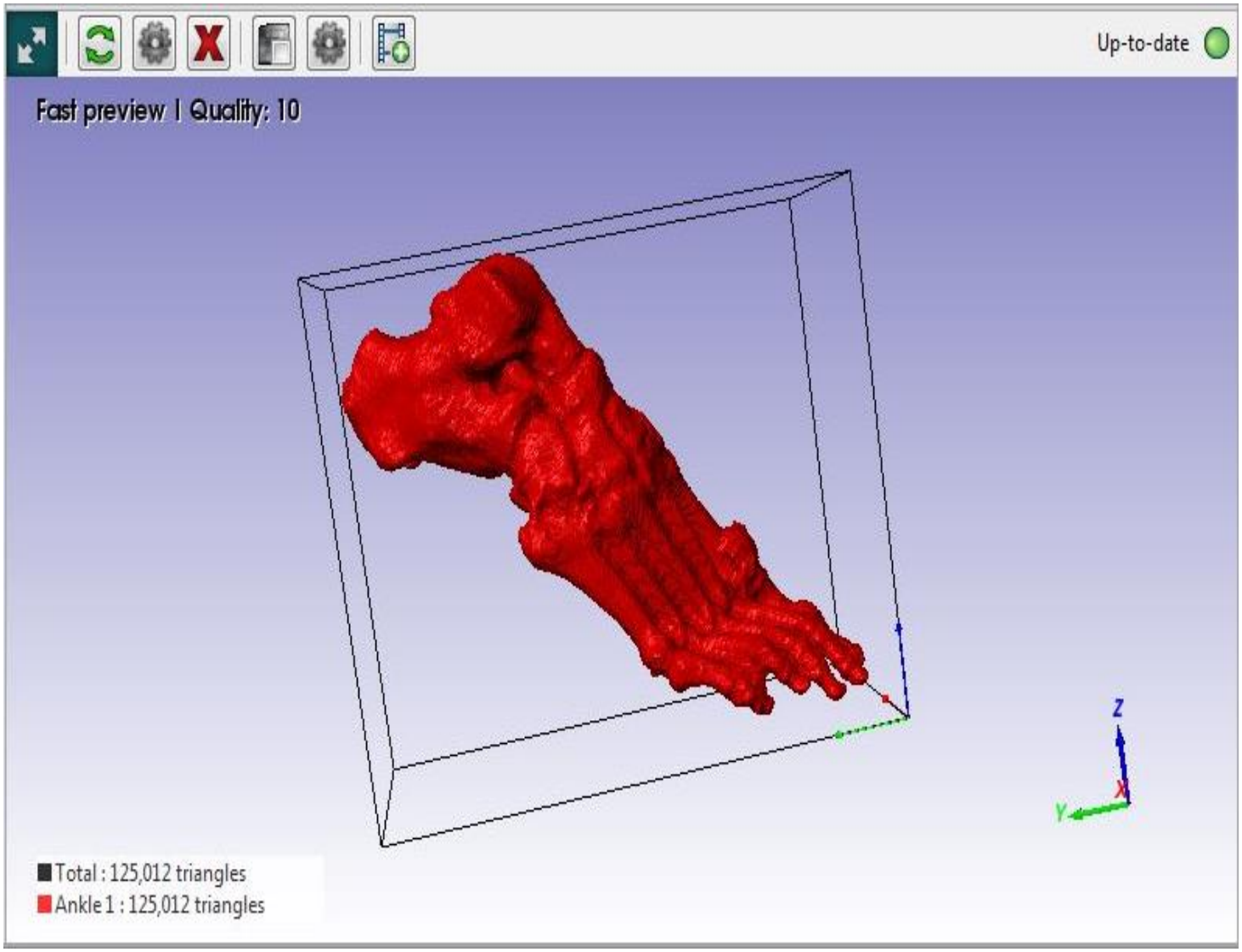


Figure 21 Application of image smoothing (Recursive Gaussian) filter and its result

Since. there are holes over the mask of the segmented femur, these holes are required to be closed prior to smoothing process. There is a requirement to apply *Close* first prior toemploying smoothing taskthat is a morphological filter. It was applied with a value of 3 (cubic values) on the present mask. Now the cavities are also filled using *Cavity Fill* filteron the active mask. After all these operations the image is smoothed by applying Recursive Gaussian filter on active mask with Gaussian sigma value as 1. A Gaussian sigma value between 1 to 3 is preffered for smoothing. In this research it was taken to be 1.

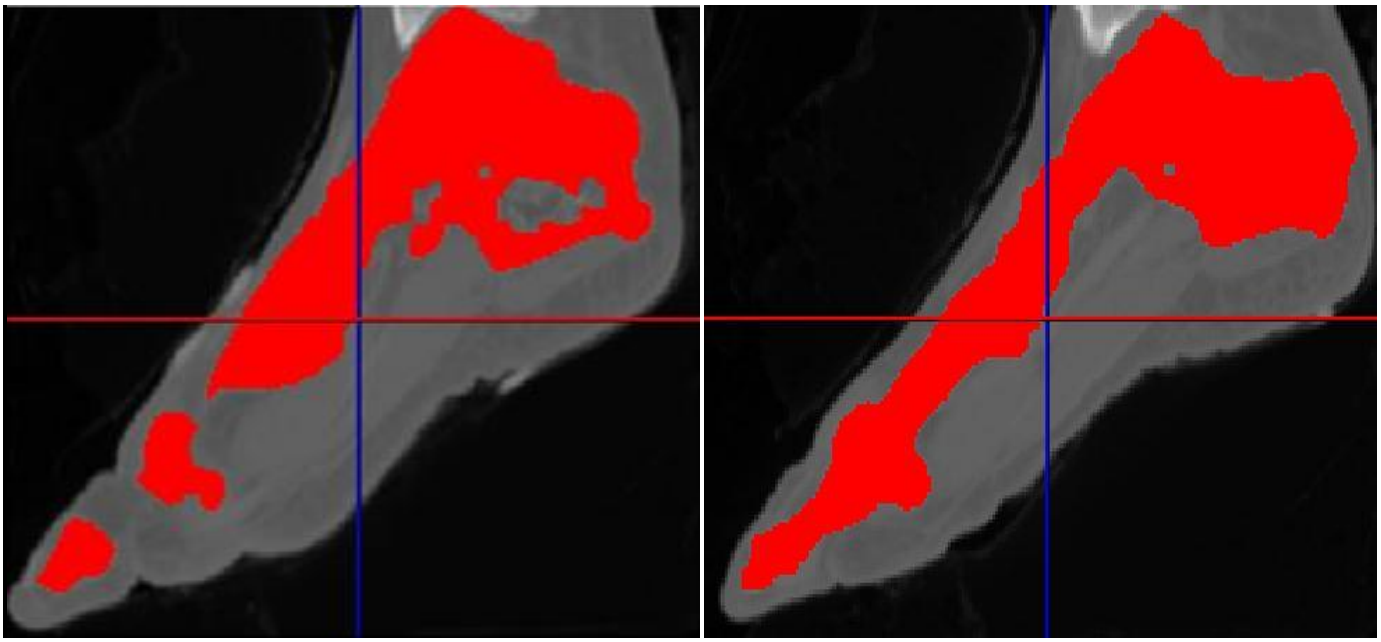

Fig. The ankle foot mask before and after the CLOSE operation

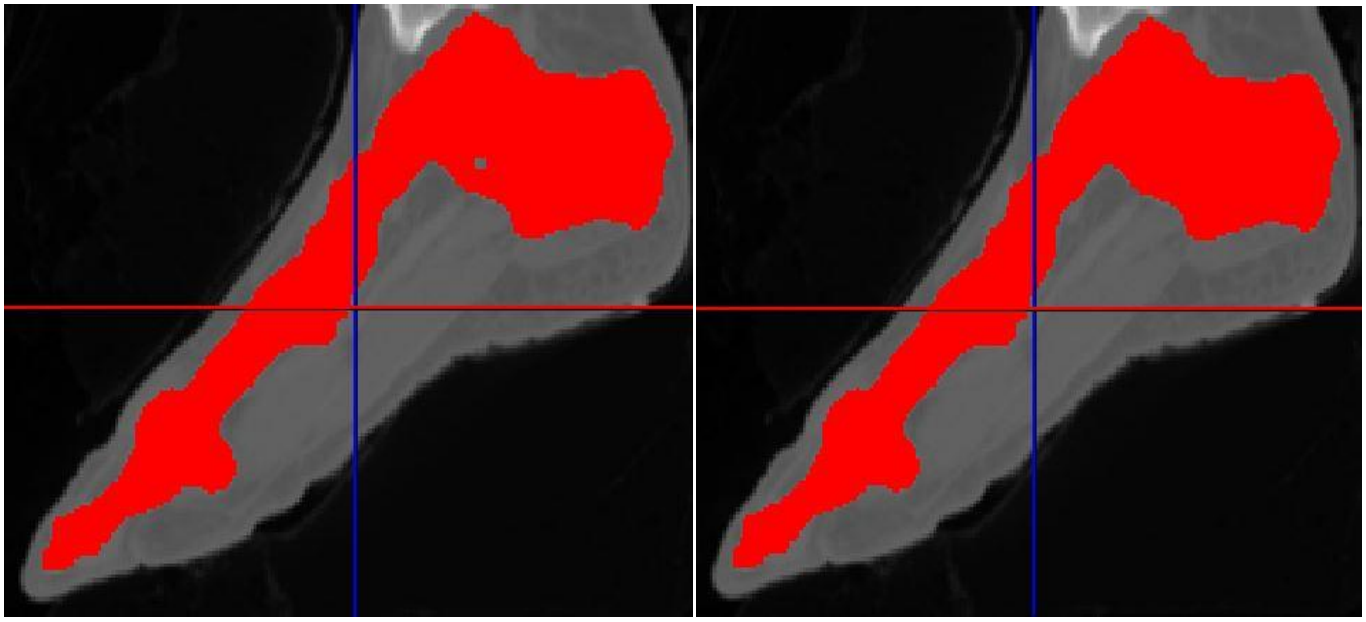

Fig. The Ankle Foot Model before and after the cavity fill operation.

Figure showing the final segmented ankle foot model after smoothing operation is shown below:

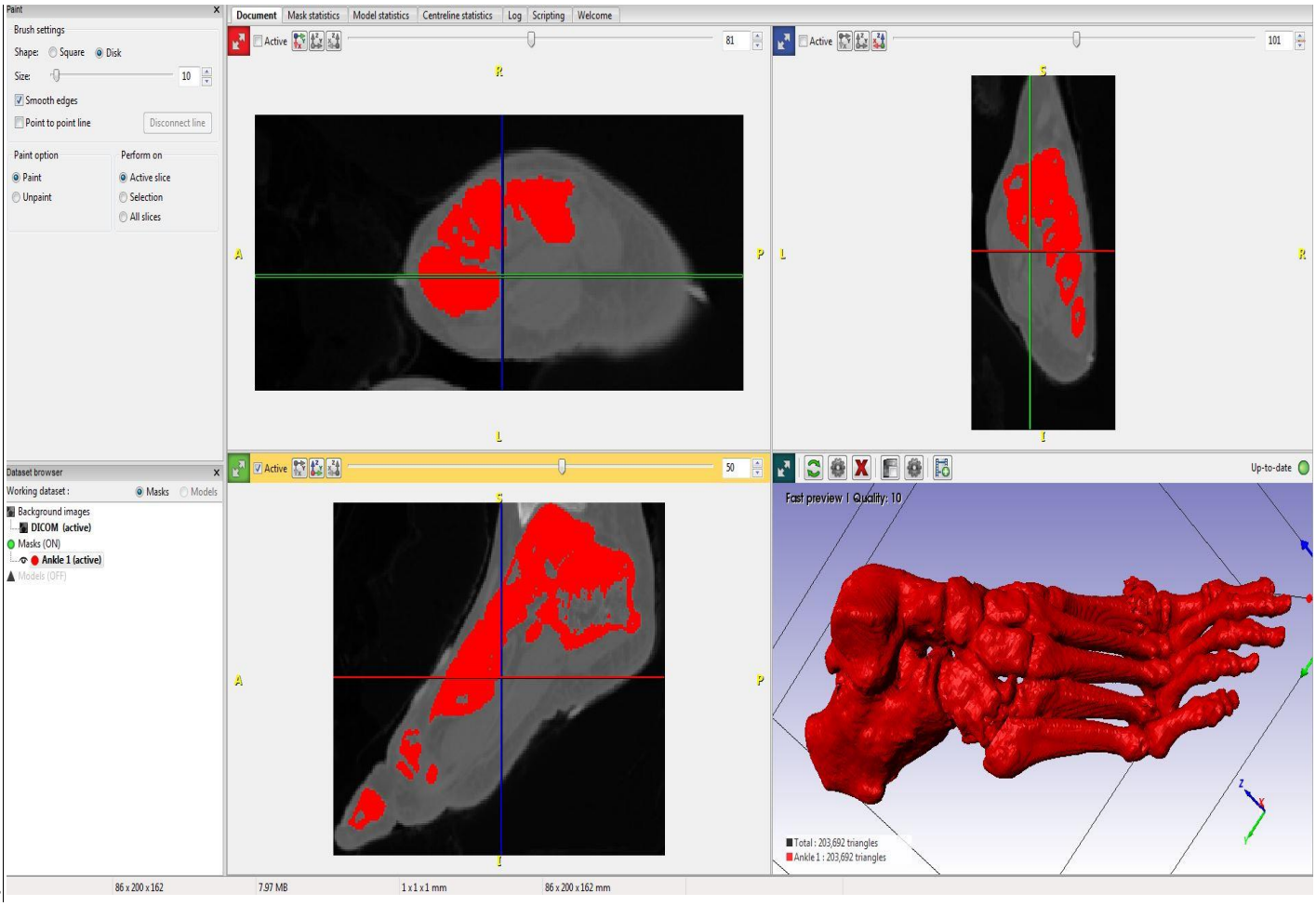


Figure 22 Final segmented Ankle Foot Model

The ankle foot model mask are now ready to be added to a NURBS model.

## 3.4 ASSEMBLY AND CONSTRUCTION OF 3D ZONES

The modelled area of interest is later converted to IGES format with transformed polygen surface to logical non-uniform b-splines surface (NURBS). These are logically described surfaces on the basis of control points [40]. The computation and description of NURBS is an important usefulness in comparison to distinct tessellated areas. In one way, this permits an improved functioning of CAD model; on the other way, the logical surfaces can be scattered like an automated hexahedral or tetrahedral meshing task can be helped. The faceted areas are transformed into NURBS appropriately; the bone can be transmitted to a pre-processor with the help of the IGES boundary. On condition that the surfaces develop a waterproof body, the solid can later be meshed with tetrahedral finite elements. It was further imported into CAD packages (SOLIDWORKS) for assembling and regeneration of knee joint.

Following steps were involved in this process:-

Prior to creating the NURBS surface, it was important to ensure that the segmented masks were properly prepared. The surface features of the geometry mainly decide the success of fitting a NURBS surface as well as the final quality of the patches. Since, the patches will attempt to surface all existing features, so, a mask with small spurious features or rough patches will reduce the quality of NURBS patches. It was important to remove any unwanted features from the segmentation as the NURBS surface fitting is feature preserving. This reduces the need to generate flawed NURBS patches and therefore reduces the possibility of NURBS algorithm failing to create a valid surface.

The morphological CLOSE filter removes any patches thereby reducing the amount of data loss in the mask whereas the Recursive Gaussian smoothing filter is used to make the mask as smooth as possible. The model for NURBS fitting is then created by successfully optimizing the segmentation and ensuring that the mask is ready and sufficiently smooth (Figure 22).

The NURBS model generation includes two major steps: Firstly, a triangulated surface was created using the parameters in the General and surface settings tab in Model Configuration tool. The triangulated surface was then used as the input to fit a NURBS surface using the parameters in NURBS fitting tab (Figure 23).

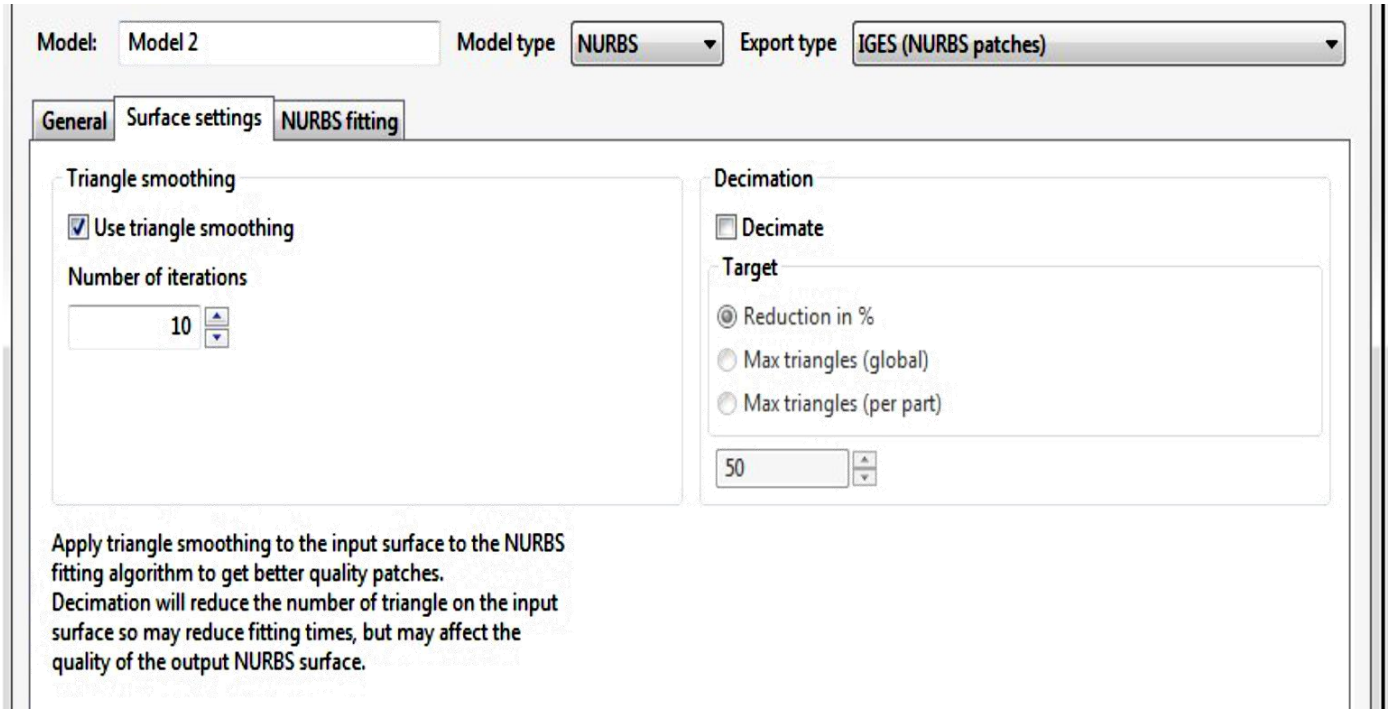


Figure 23 Window showing surface fitting parameters in Model Configuration tool.

The NURBS surface was created, successfully configured and then inspected to focus on locating small surface artefacts that if left would cause NURBS algorithm to fail or produce invalid NURBS patches. The level of triangle smoothing was increased and the surface model was regenerated if such artefacts were present (Figure 23).

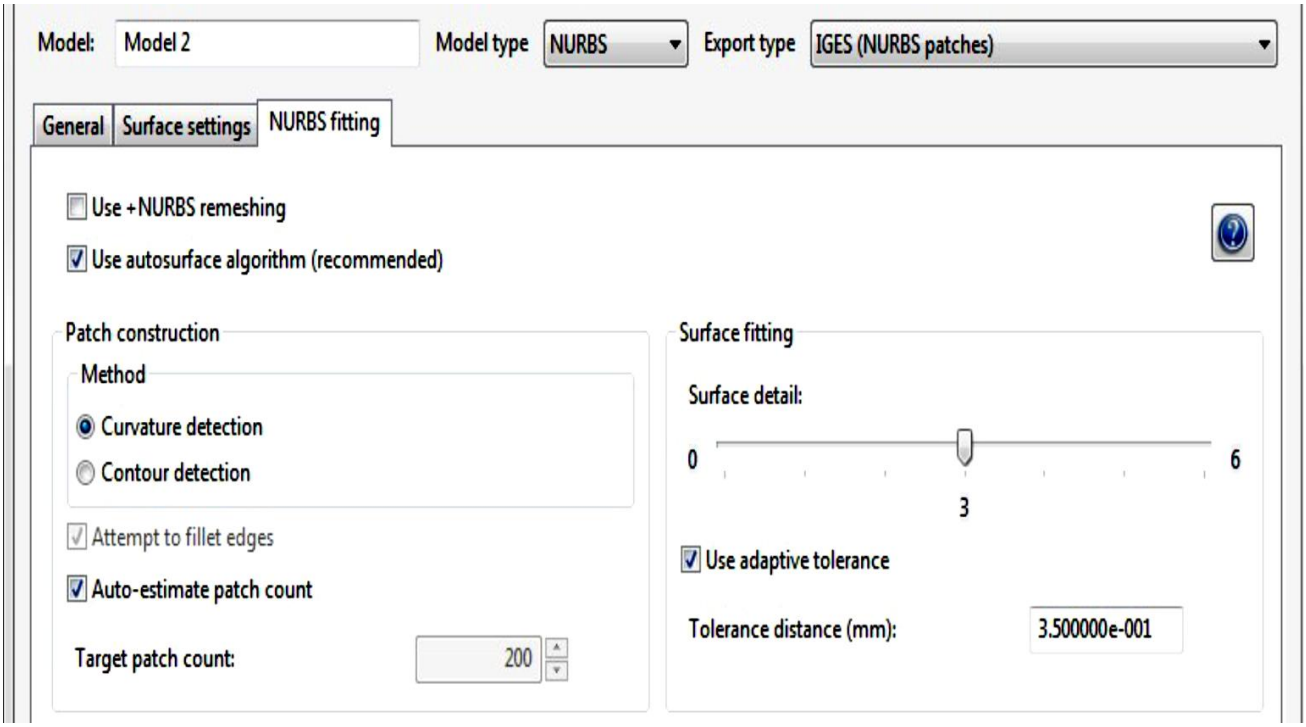


Figure 24 Window showing NURBS fitting parameters in Model Configuration tool.

NURBS model preview was generated to create the triangulated (i.e. STL) mesh (Figure 24). The generated surface model was inspected to check the smoothing settings and segmentation quality. It was then required to launch the NURBS algorithm. Finally, solid (NURBS) model/ FE model of ankle foot model was generated and exported in IGES format (Figure 25).

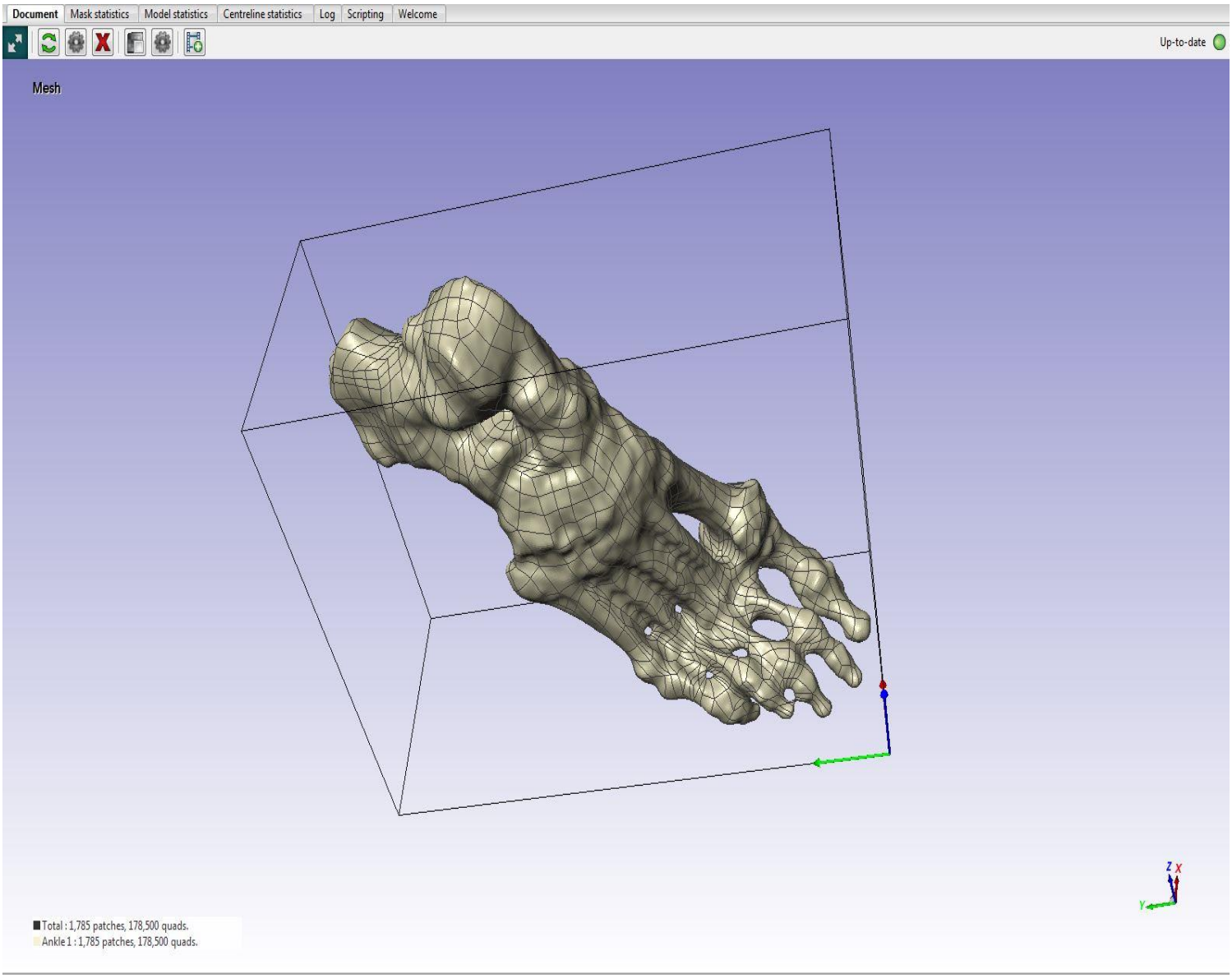


Figure 25 A sneak of the NURBS surface model

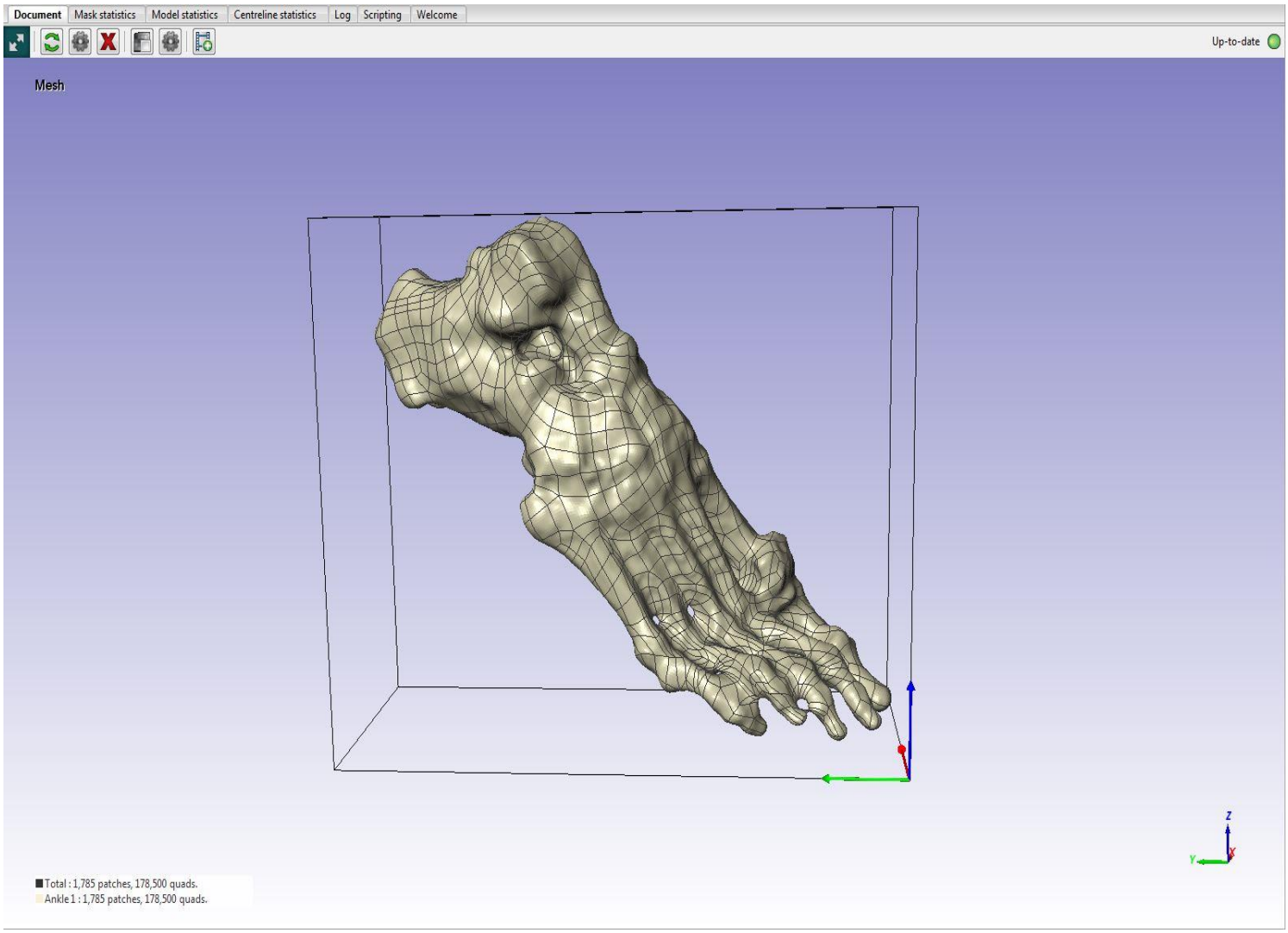


Figure 26 A sneak of the NURBS surface model

# CHAPTER 4

# FINITE ELEMENT ANALYSIS

## 4.1 FINITE ELEMENT ANALYSIS

Finite Element Analysis (FEA) is an analysis tool in engineering, with applications in static, dynamic, buckling, thermal, linear, non-linear, structural and fatigue analysis. It's an approx. numerical technique which gives mathematical analysis of actual problem. For load carrying structures of unlimited complexity FEA is used to calculate stresses, although there are limitations of a practical nature. All above the method is suited for stress analyses of irregular components as bon-prosthesis structures and is increasing interest in biomechanics research [34], [35], [32].

Minimum number of parameters (motion, coordinates, temp. etc.) required to define position of any entity completely in the space is known as degree of freedom (dof). Any continuous object has infinite degrees of freedom & it's not possible to solve the problem. So, basic theme of FEA is to make calculations at limited (finite) no of points & then interpolate the results for entire domain (surface or volume). Therefore, FEM reduces degree of freedom from infinite to finite with the help of discretization, i.e., meshing (nodes & elements) [36]. Elements are the basic building blocks such as

triangle, quadrilateral, tetrahedrons & bricks. Mesh is the collection of elements and nodes are the corners where a number of elements meet.

### 4.1.1 HISTORY OF FEA

In 1943, R. Courant was the first to give a mathematical foundation for present form of FEA by utilizing the Ritz method of numerical analysis and minimization of variational calculus to obtain approximate solutions to vibration systems. Soon afterwards, M. J. Turner, R. W. Clough, H. C. Martin, and L. J. Topp published a paper entitled “stiffness and deflection of complex structures” in 1956 which established a broader definition of numerical analysis. In the late 60’s, mechanical industry recognized FEA as useful tool for solving real life problems. By the early 70's, FEA was limited to expensive mainframe computers generally owned by the aeronautics, automotive, defense, and nuclear industries. In 1972, Brekelmans et al. published a paper titled “new method to analyze the mechanical behavior of skeletal parts”, was first introduced in the orthopedic literature after about fifteen years when the finite element method (FEM) initiated a revolution in stress analyses of structure in engineering mechanics. In later

1980’s, graphical and computational development took place. Since 1990’s FEA has been developed to an incredible precision due to the advent of low cost computers and exceptional increase in computing power [36], [37].

### 4.1.2. STEPS INVOLVED IN FEA

An analyst can obtain a solution for the stress and strain distribution throughout a continuum when the applied loads, boundary conditions and material properties are known with the help of FE method. The basic steps in any software based finite element analysis consist of the following [36], [38]:

a) Preprocessing Phase

b) Creating a 3D CAD Model: Use any of the 3D CAD modeling tools like ProE, Catia, Creo and solid Edge etc. for creating the 3D geometry of the part/assembly of which you want to perform FEA.

c) Importing 3D CAD geometry to FEA Package: Start the FEA package and import the CAD geometry into the FEA package like Abaqus, Ansys, and Nastran.

d) Defining Material Properties: Define material which is going to be used for the part/assembly in FEA package. By this process, one can define modulus of elasticity, Poisson's ratio and all other necessary properties required for the FEA.

e) Meshing: Meshing is a fundamental step in FEA. In this operation, discretization is used to convert infinite dof to finite elements. So, after this operation the CAD geometry is divided into large numbers of small elements. The small elements are called mesh. The analysis, accuracy and duration depend on the mesh size and orientations. With the increase in mesh size, the finite element analysis speed increases but the accuracy decreases.

f) Defining Boundary Condition: Boundary conditions are the loads and constraints that represent the effects of the surrounding environment on the model. Loads can be forces, moments, pressures, temperatures, accelerations and constraints are for resist the deformations induced by the loads. So, by defining where loads applied and where constraints applied to rest the part/assembly.

After completion of preprocessing, software internally forms mathematical equations in the form

$$\{F\} = [K]\{\delta\} \tag{2}$$

where, {F} is the vector of applied nodal forces, [K] is a square matrix, known as the stiffness matrix, and {δ} is the vector of (unknown) nodal displacements.

b) Solution Phase

In this step, FEA package solve the problem for the defined material properties, boundary conditions and mesh size. Internally, software carries out matrix formation, inversion, multiplication & solution for unknown, such as displacement & then finds strain & stress for static analysis.

The solution is obtained numerically through a set of linear equations, equal to the amount of degrees of freedom in the model: the number of nodal points times the number of displacement components in each node (two in a 2-D, three in a 3-D model). The processing time and memory space required for a problem in computer progressively depends on the number of degree of freedom. A time-efficient element mesh is crucially important, since computer hardware capacity is the only practical limit to the level of model complexity feasible.

c) Post processing Phase

In this step, FEA package gives results of the solution. The result can be viewed in various formats like graph, value, animation etc. through which you can verify, conclude and think what steps could be taken to improve the design.

### 4.1.3 ADVANTAGES OF FEA

a) Increases visualization: It is not easy to visualize or predict failure location for real life complex problems but with the help of this tool one can successfully predict failure location for the given set of forces.

b) Decrease design cycle time: Conventional chain design cycle is a very long & time consuming process while current concurrent engineering design cycle is very fast & more efficient due to which design cycle time is decreased.

c) Optimum design: It provides most appropriate environment which results into a favorable design outcome.

### 4.1.4 ANSYS

ANSYS is a widely used finite element analysis package which can simulate problems in area of structural mechanics, electromagnetics, heat transfer, fluid dynamics, acoustics and coupled problems. It has the capability to analyze static and dynamic, linear and non-linear problems in structural analysis. The simulations carried out in this work are linear static in nature.

Linear static analysis is the most basic type of analysis. The term “linear” signifies that the computed response (displacement, stress or strain) is linearly related to the applied force. And the term “static” signifies that there is no variation of forces with respect to the time or, that the time variation is insignificant and can therefore be safely ignored [39].

**4.2 MATERIAL PROPERTIES USED**

Bone behavior was approximated by a homogeneous isotropic linear elastic material. The average mechanical properties of each type of bone tissue are shown in Table 1which was extracted from CES selector (Cambridge Engineering Selector, an engineering materials selection tool). The lower boundary of the bone properties was selected for these simulations because most of the patient which undergoes TKA is elderly having problem of bone degradation or osteoporosis which weakens the mechanical property of bone.

| Structural Properties Of Bone | Value |
|---|---|
| Young's Modulus | 1.7e10 Pa |
| Poisson's Ratio | 0.30 |
| Density | 1.9e3 kg/m³ |
| Thermal Expansion | 1e-5 /°C |
| Tensile Yield Strength | 1.2e8 Pa |
| Compressive Yield Strength | 1.1e8 Pa |
| Bulk Modulus | 1.8e10 Pa |

**Table 1** *Table of the material properties of bone*

**4.3 BOUNDARY CONDITIONS**

Fig. 1.5 shows the heel-strike of foot during normal walking. In the first step heel strikes the ground. In the second step the mid-foot makes contact and in the third step forefoot remains in contact. Majority of runners have encountered in the clinic run, rear foot striking pattern during which initial contact occurs at the heel. These individuals also tend to demonstrate longer strides, decreased stride rates , and experience greater impact peaks of ground reaction forces (GRF) at initial contact. Research has shown that power absorption of lower extremity in these runners occurs primarily at the knee[13].These individuals will commonly experience anterior knee pain, tibial stress fractures, lower back pain, and plantar fasciitis. With the recent emergence of the “barefoot running craze”, there is an increasing number of individuals who demonstrate a forefoot striking pattern. Runners with this type of style demonstarte initial contact closer to the lateral ball, of their foot, shorter stride lengths, increased stride rates, and experience less impact peaks of GRF. These individuals typically present with Achilles tendonitis, calf strains, metatarsal stress fracture, and foot pain [13].Angle variation of different foot strike pattern was shown in Fig.26.

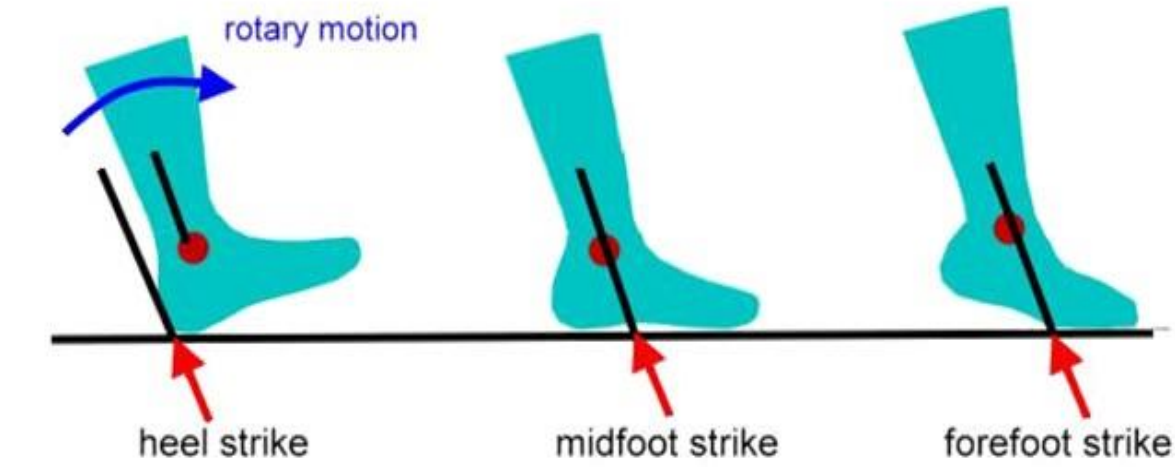


**Fig. 27** *Different foot strike patterns[14]*

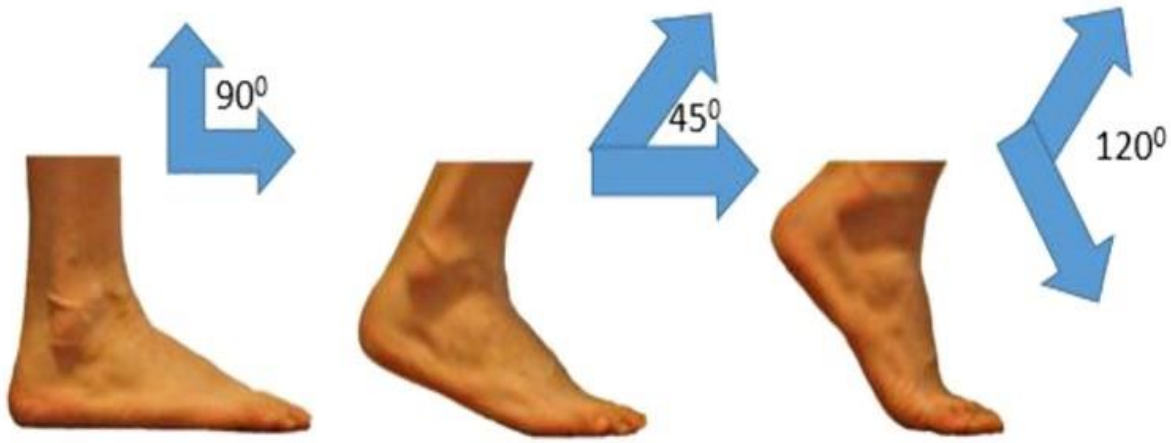


**Fig. 28** *Angle varies between different foot strike patterns*

In Fig.27 the line of gravity and contact point of the foot was shown in standing condition. Here the contact point was in the middle of the foot. The center of gravity varies according to the position and orientation of foot. The three planes of foot, frontal plane, sagittal plane and the transverse plane was shown in Fig. 28. The frontal plane passes through the ankle joint and is parallel to the media-lateral direction. The sagittal plane passes through the ankle joint and is parallel to the longitudinal plane of the body. The transverse plane is parallel to the ground. The sequence of segmented CT images of the foot obtained is shown in Fig. 29 below. From the processed CT images the foot model was reconstructed with the use of various segmentation techniques.

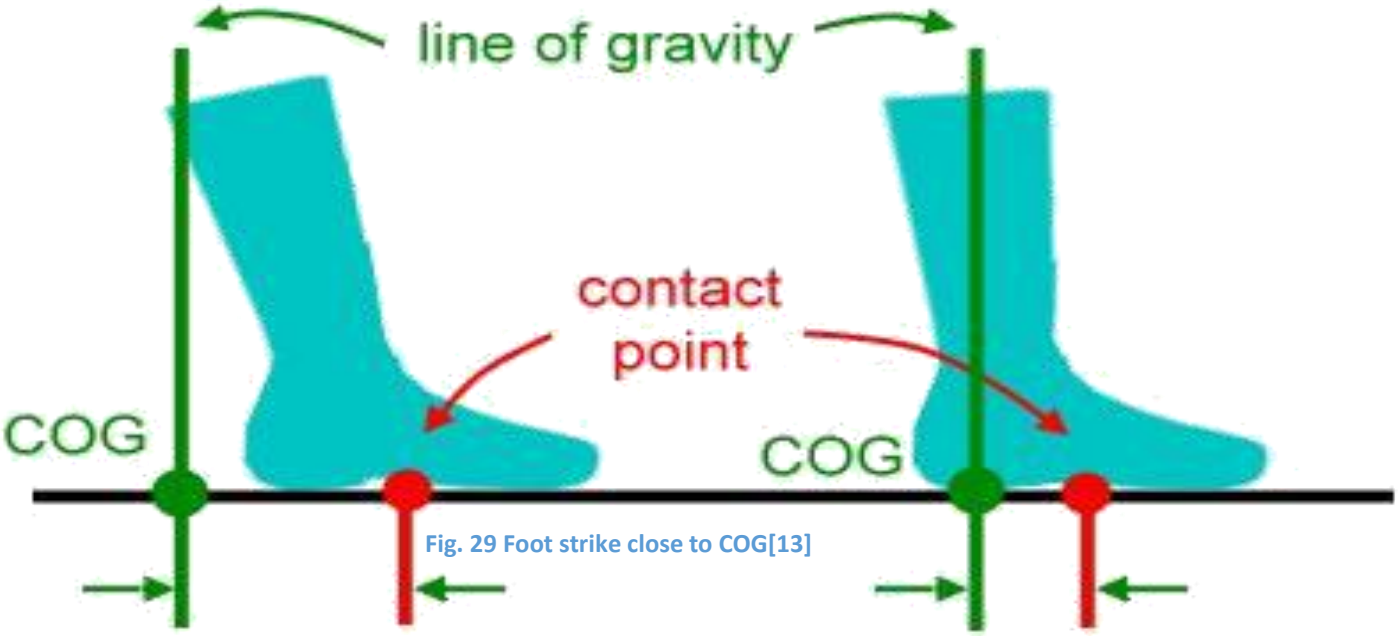


Fig. 29 Foot strike close to COG[13]

Boundary condition is applied to the meshed model and post processing is done. Various loads have been applied along different directions. Three different load angle was chosen (at an angle of $90^0$, $120^0$, $45^0$). The angle is so chosen as during normal walking on a flat surface, the load on the foot has an angle of $90^0$ with the horizontal. During ascending or climbing a slope the load on the foot is assumed to have an angle of $45^0$. Similarly, while descending a slope the load on the foot is assumed to have an angle of $120^0$. Three different loads such as 600N,700N and 800N was applied for each angle. At 90 degree the load was also applied in a direction normal to ground (horizontal). The total deformations of the model were calculated. The maximum total deformation was observed to be $7.948e^{-5}$(.053553 m) and minimum was found to be 0 shown in Fig. 29.

# CHAPTER 5

# RESULTS AND DISCUSSION

The following results were obtained during this project. The 3D model of human foot bone was developed using various software tools. First the combined image was obtained from CT scan images. Then a 3D model was constructed from the 2D image. Then it was cleaned. After cleaning it was imported into ANSYS for analysis.

Boundary condition is applied to the meshed model in ANSYS and post processing is done. Various loads have been applied along different directions. Three different load angles were chosen (at an angle of $90^0$, $120^0$, $45^0$). The angle is so chosen as during normal walking on a flat surface, the load on the foot has an angle of $90^0$ with the horizontal. During ascending or climbing a slope the load on the foot is assumed to have an angle of $45^0$. Similarly, while descending a slope the load on the foot is assumed to have an angle of $120^0$. Three different loads such as 600N, 700N and 800N were applied for each angle. At 90 degree the load was also applied in a direction normal to ground (horizontal). The total deformations of the model were calculated. The maximum total deformation was observed to be $7.948e^{-5}$(.053553 m)and minimum was found to be 0 shown in Fig. 5.1.

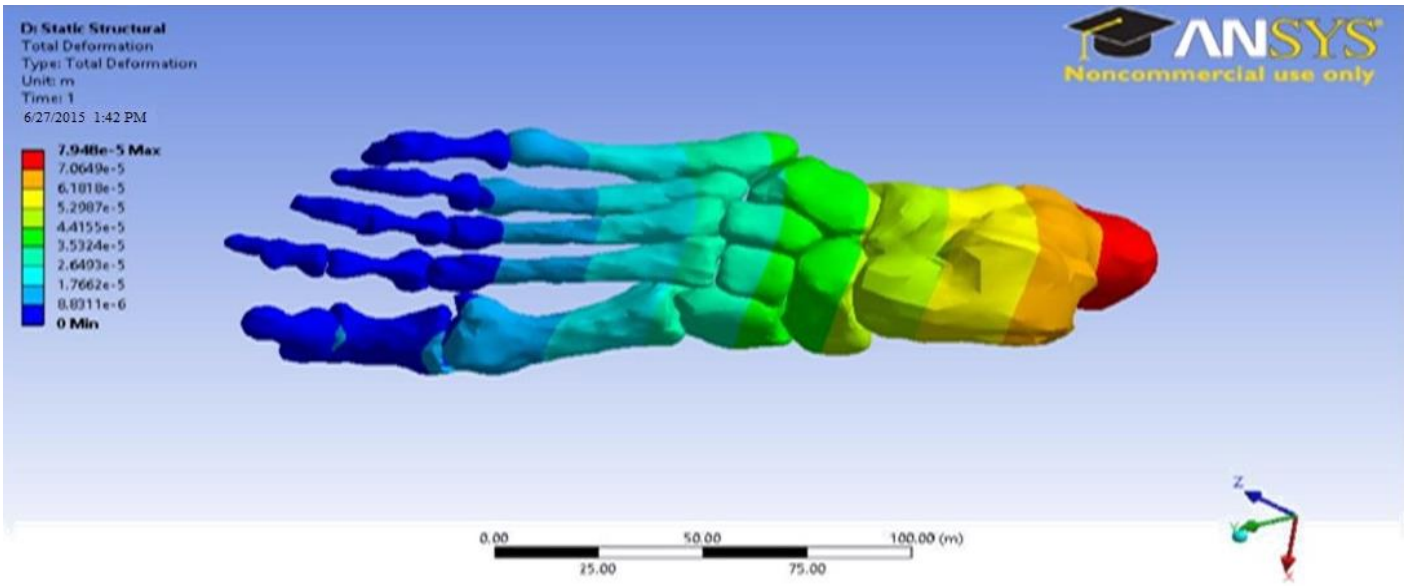


**Fig. 5.1** *Screenshot of total deformation of foot model by applying 600 N at an angle of $90^0$*

Secondly, 700 N force was applied in a direction normal to ground. The maximum total deformation was observed and it was found to be $9.2726e^{-5}$(.062478m). The minimum deformation was found to be 0 as shown in Fig. 5.2.

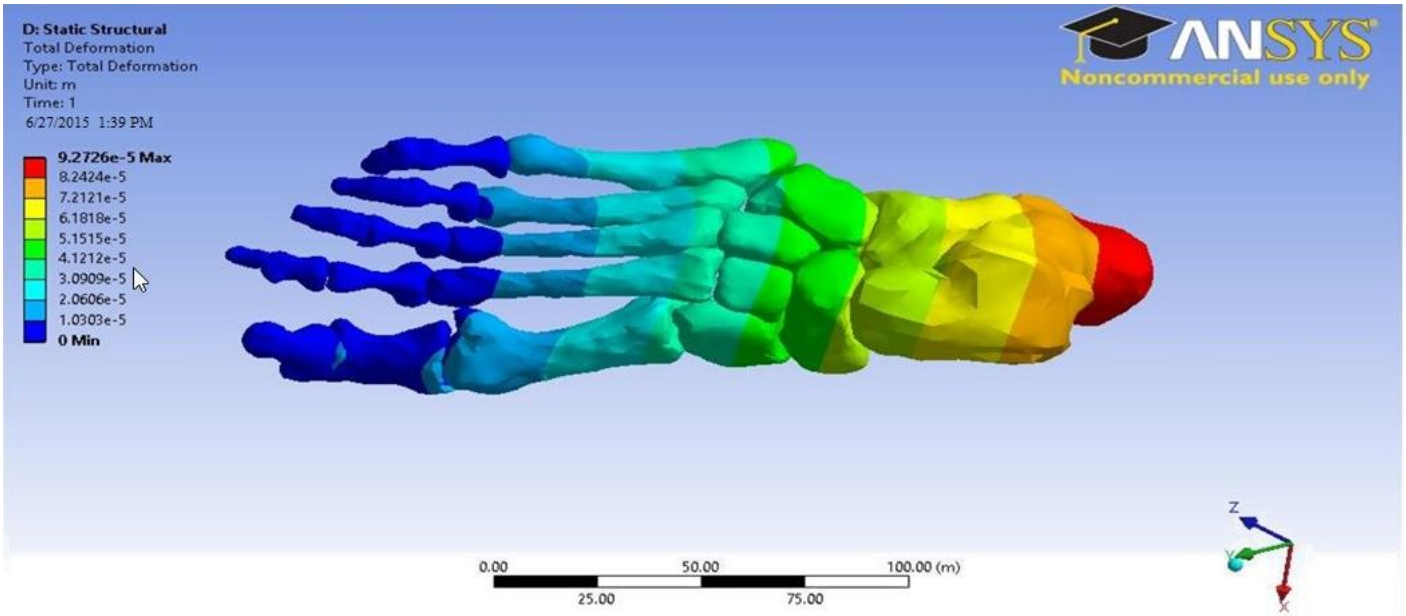


**Fig. 5.2** *Screenshot of total deformation of foot model by applying 700 N at an angle of $90^0$*

Finally, 800 N force was applied normal towards the horizontal. The maximum total deformation was observed and it was found to be $9.935e^{-5}$(.066941m) and the minimum was found to be 0 as shown in Fig. 5.3.

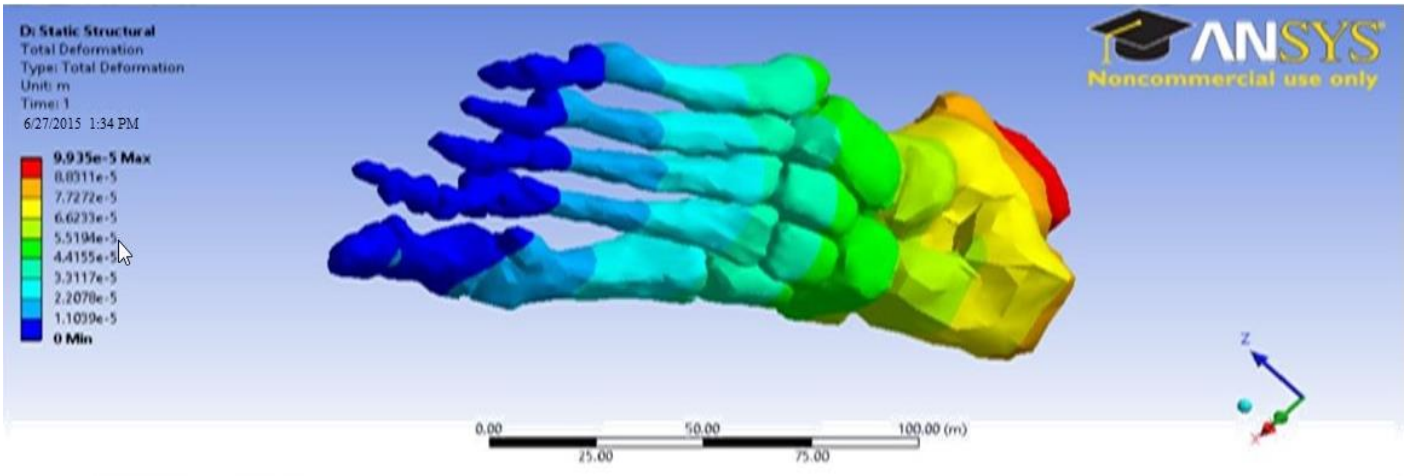


**Fig. 5.3** *Screenshot of total deformation of foot model by applying 800Nat an angle of $90^0$*

Then total deformation was calculated at $120^0$ angle. First 600N was applied. The maximum deformation was found to be $3.83e^{-5}$(0.025806 m) and the minimum deformation was 0 as shown in Fig. 5.4.

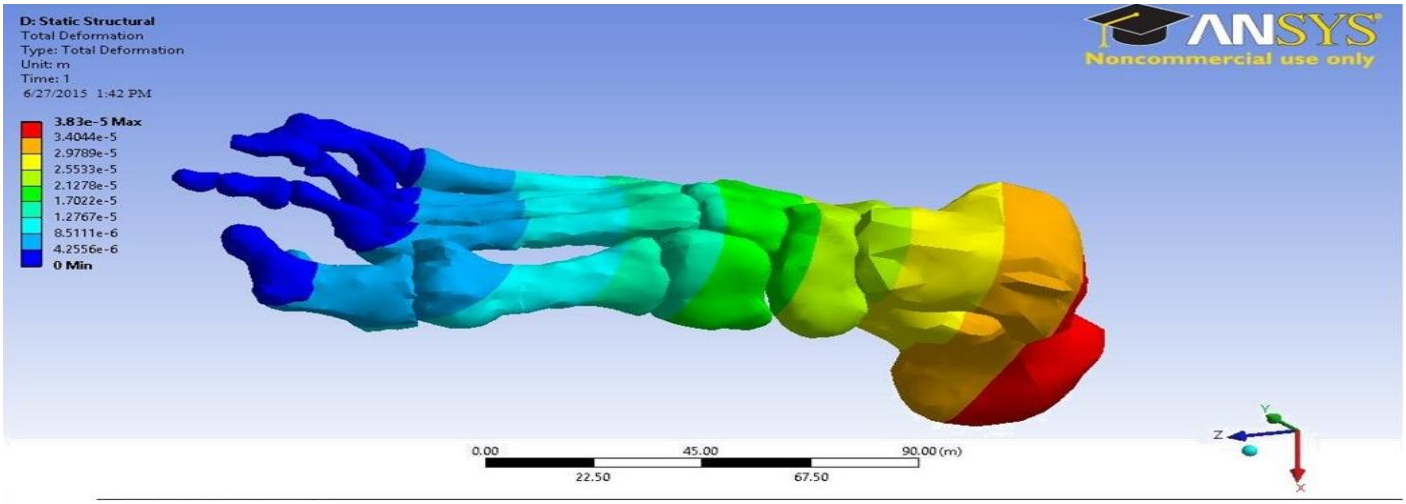


**Fig. 5.4** *Screenshot of total deformation of foot model by applying 600Nat an angle $120^0$*

By applying 700N, the maximum deformation was found to be $4.4683e^{-5}$(0.030107 m) and minimum was 0 as shown in Fig. 5.5.

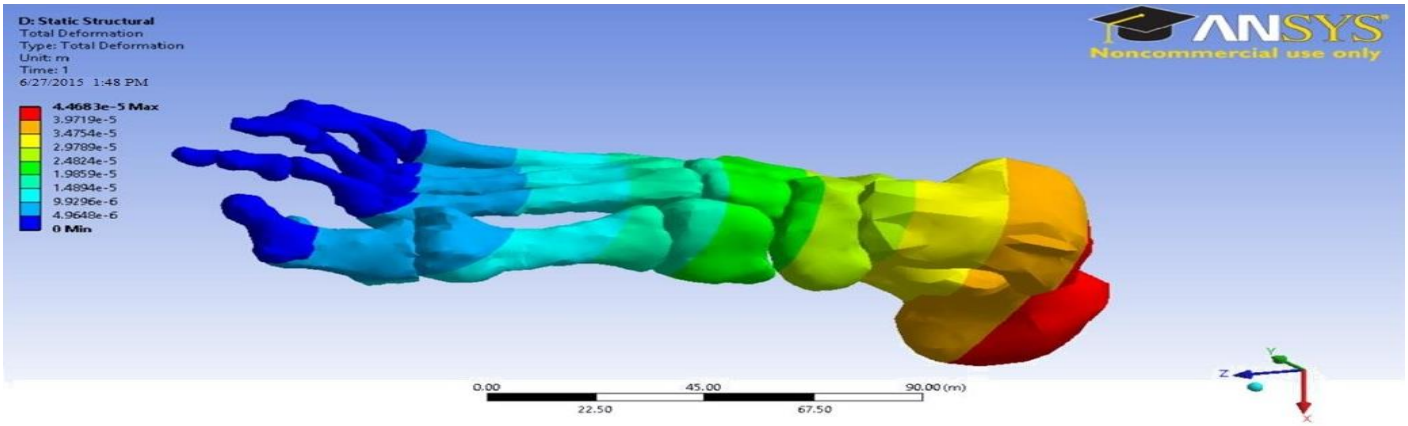


**Fig. 5.5** *Screenshot of total deformation of foot model by applying 700Nat an angle $120^0$*

By applying 800N maximum deformation was found to be $5.1067e^{-5}$(0.034408 m) and the minimum deformation was 0 as shown in Fig. 5.6.

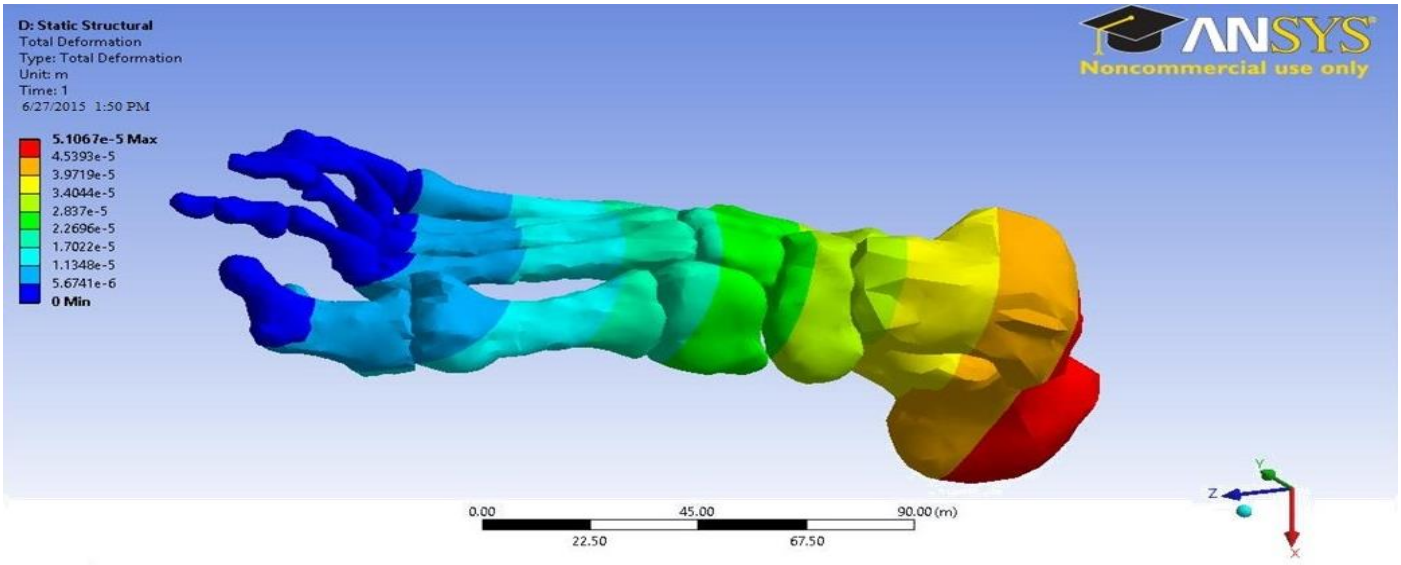


**Fig. 5.6** *Screenshot of total deformation of foot model by applying 800Nat an angle $120^0$*

Finally the deformation was calculated for $45^0$ angles. The maximum deformation was found to be $5.8855e^{-5}$ (0.039656 m) by applying force of 600N as shown in Fig. 5.7.

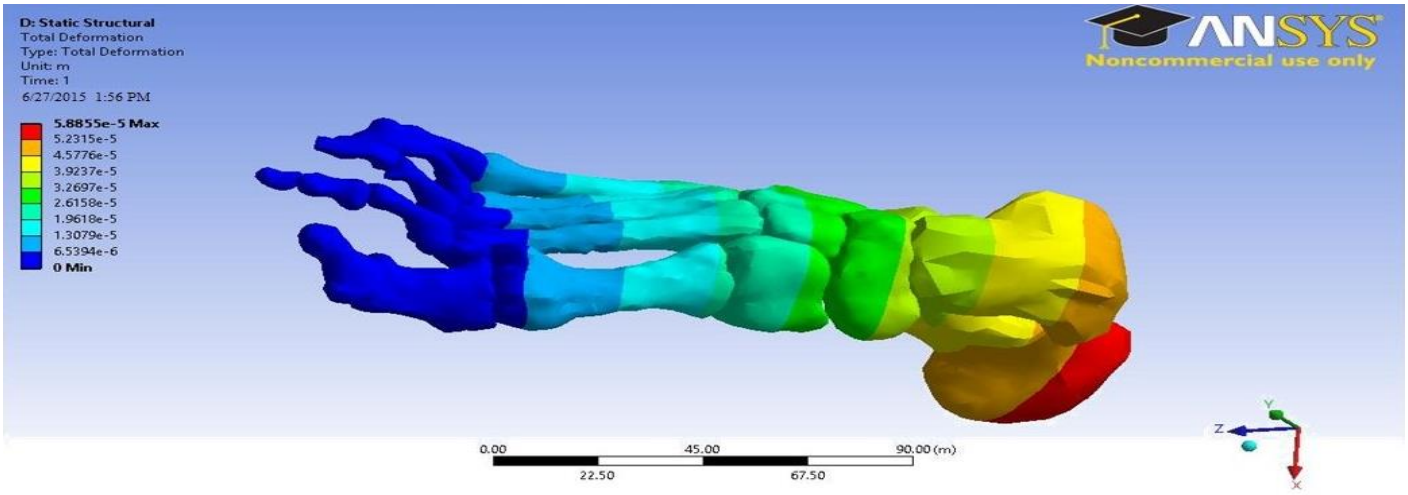


**Fig. 5.7** *Screenshot of total deformation of foot model by applying 600N at an angle $45^0$*

By applying700N, the maximum deformation was found to be $6.866e^{-5}$**(**0.046262 m**)** and the minimum deformation was found to be 0 as shown in Fig. 5.8.

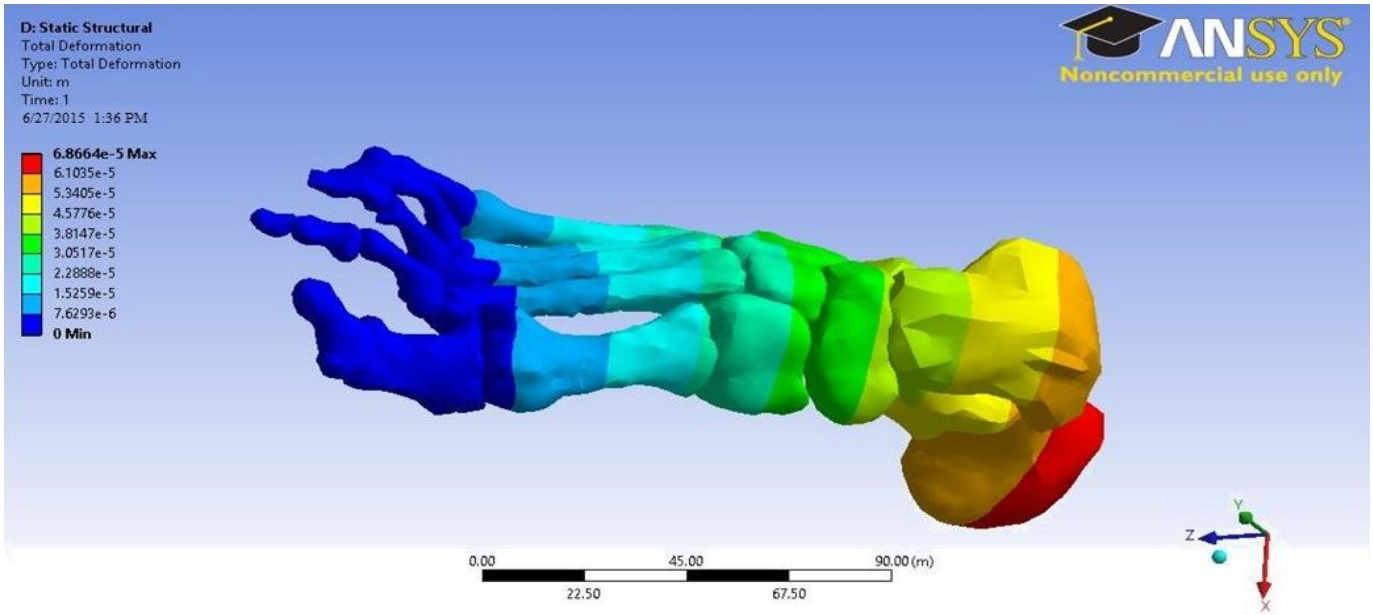


**Fig. 5.8** *Screenshot of total deformation of foot model by applying 700Nat an angle $45^0$*

By applying 800N, the maximum deformation was found to be $7.8473e^{-5}$ (0.052874 m) and the minimum deformation was found to be 0 as shown in Fig. 5.9.

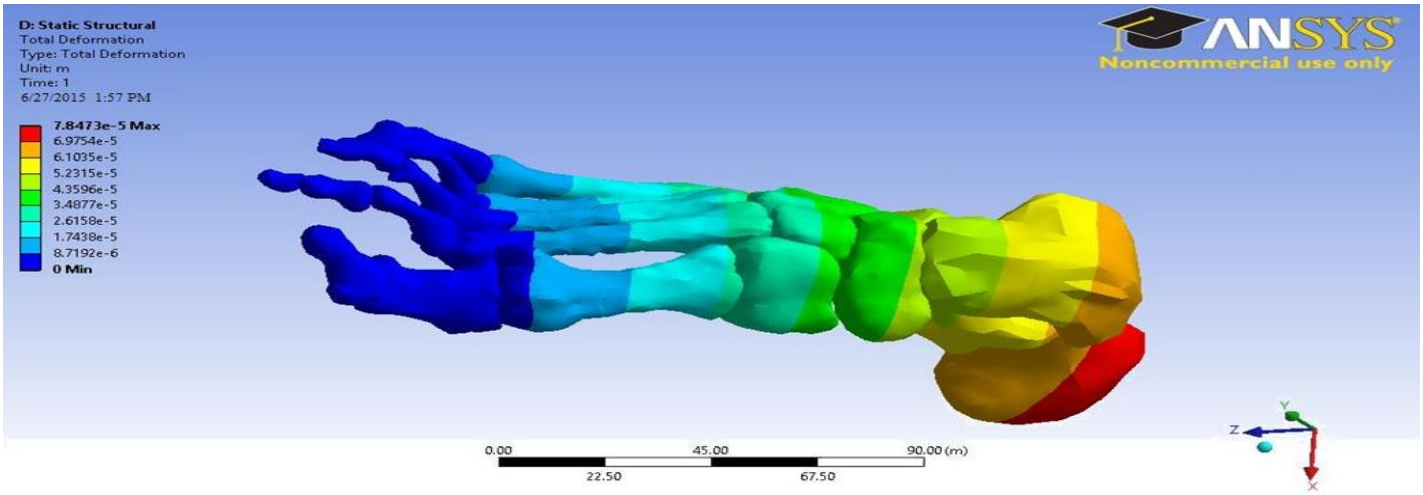


**Fig. 5.9** *Screenshot of total deformation of foot model by applying 800N at an angle $45^0$*

Similarly, Von-Mises stress was calculated by applying 600 N and 700 N (Fig 5.10 and Fig 5.11 respectively) at an angle $90^0$. The maximum stress was found to be 978.66Pa and 1141.8Pa for 600N and 700N force respectively. In all the cases forces are applied normal to ground.

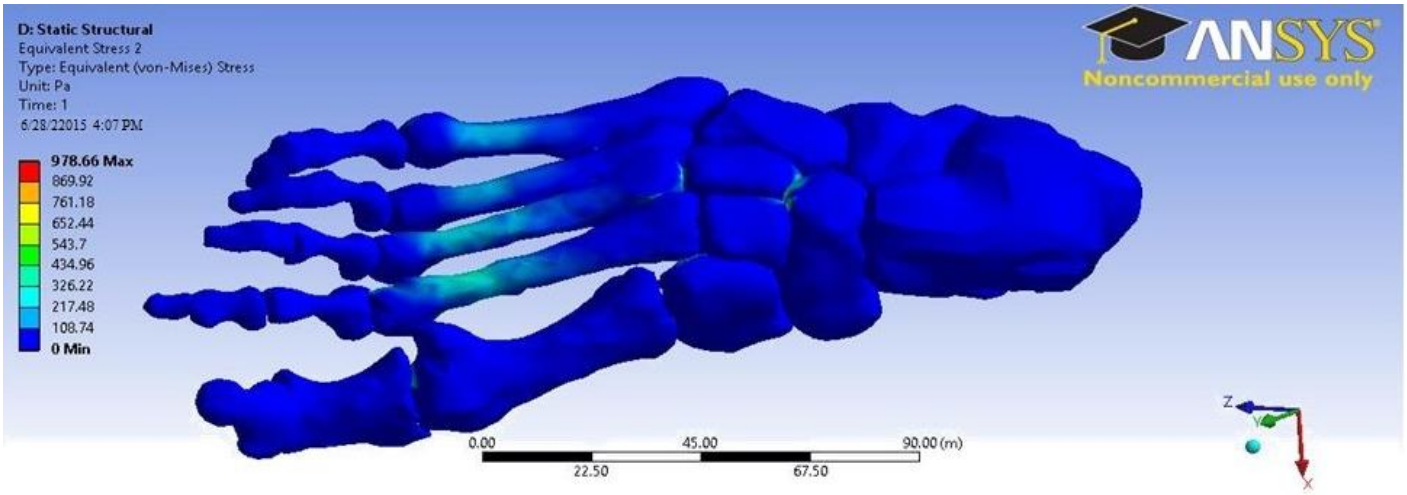


**Fig. 5.10** *Screenshot of Von-Mises stress of foot model by applying 600N at an angle $90^0$*

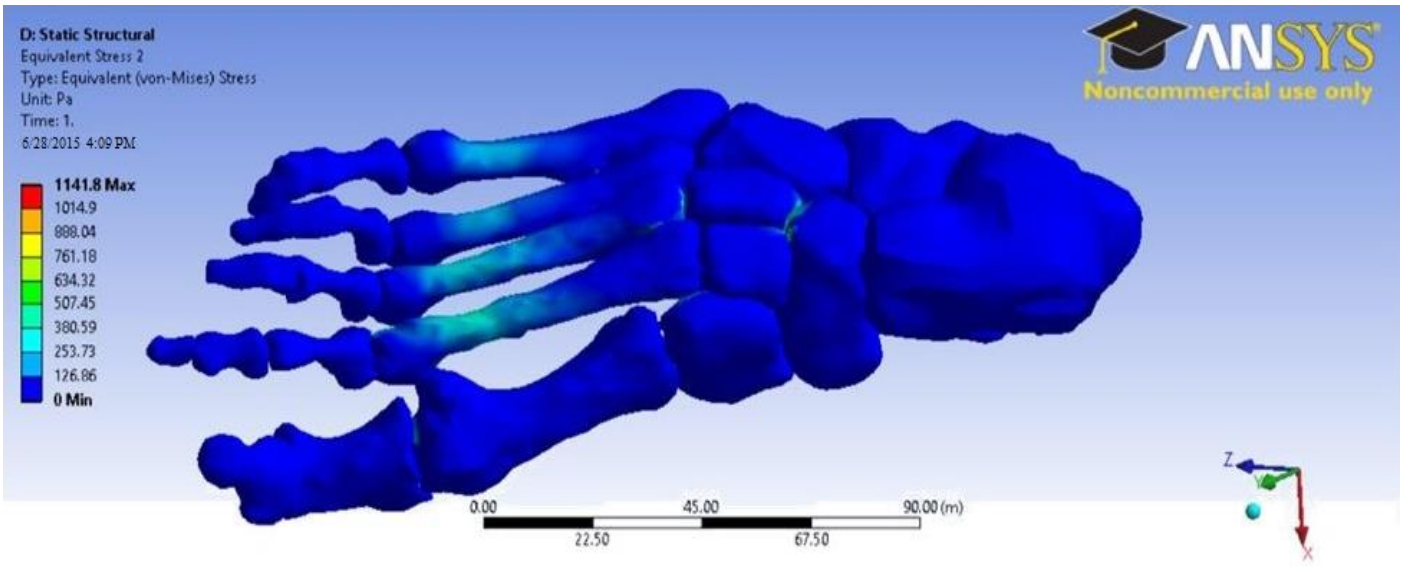


**Fig. 5.11** *Screenshot of Von-Mises stress of foot model by applying 700N at an angle $90^0$*

Finally, Von-Mises stress was calculated by applying 800 N. The numerical values of maximum Von-Mises stress were found to be at a maximum of 1304.9 Pa and minimum of 0 as shown in Fig. 5.12.

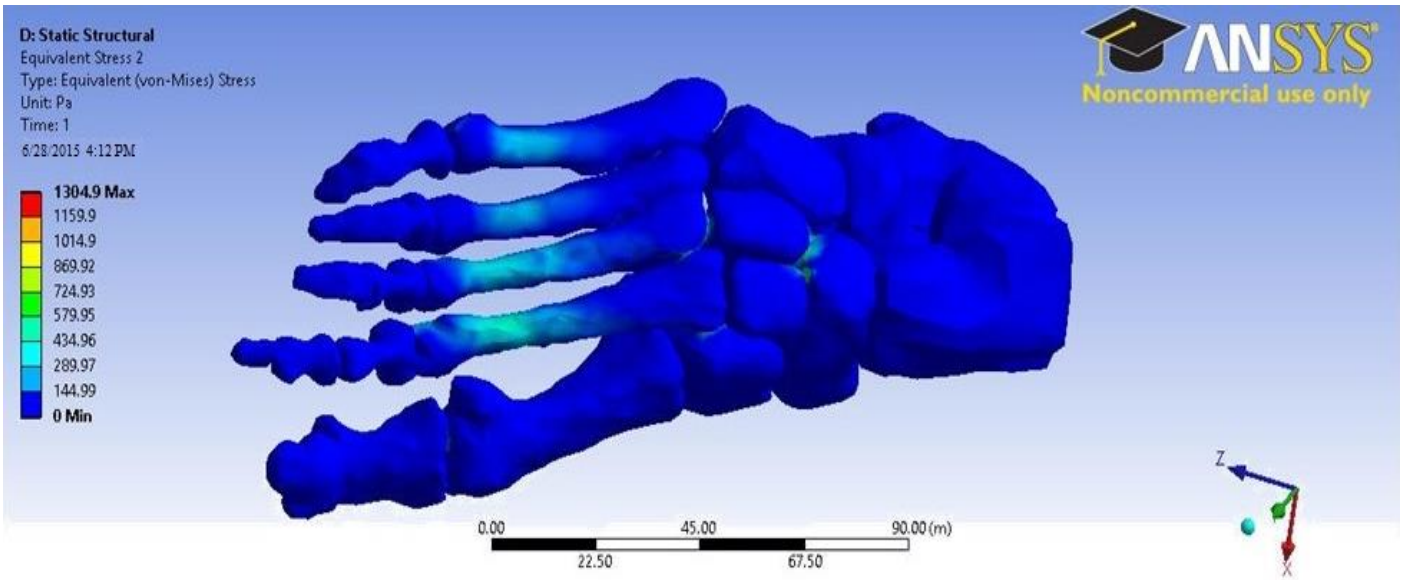


**Fig. 5.12** *Screenshot of Von-Mises stress of foot model by applying 800N at an angle $90^0$*

By applying 600N at angle of $120^0$ the Von-Mises stress was found to be 459.99 Pa as shown in Fig. 5.13. From the colour distortion in the figure it is observed that the stress value is very less.

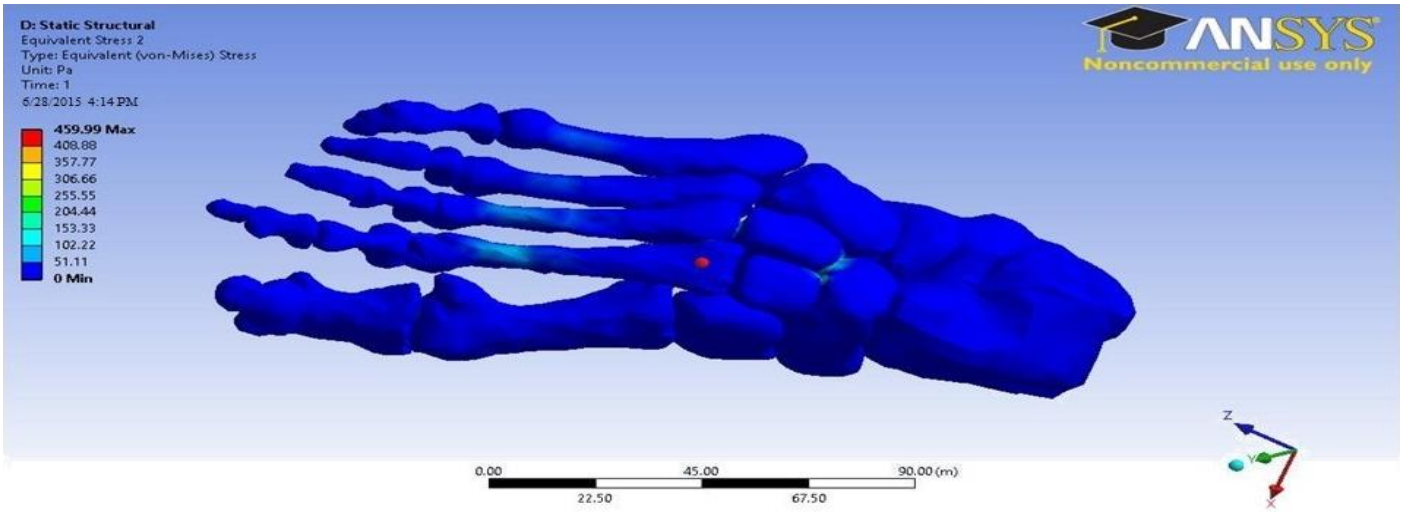


**Fig. 5.13** *Screenshot of Von-Mises stress of foot model by applying 600Nat an angle $120^0$*

Similarly, by applying 700N at angle of $120^0$ the maximum Von-Mises stress was found to be 536.66 Pa and the minimum Von-Mises stress was 0 as shown in Fig. 5.14. In this case also the observed region of colour distortion is limited.

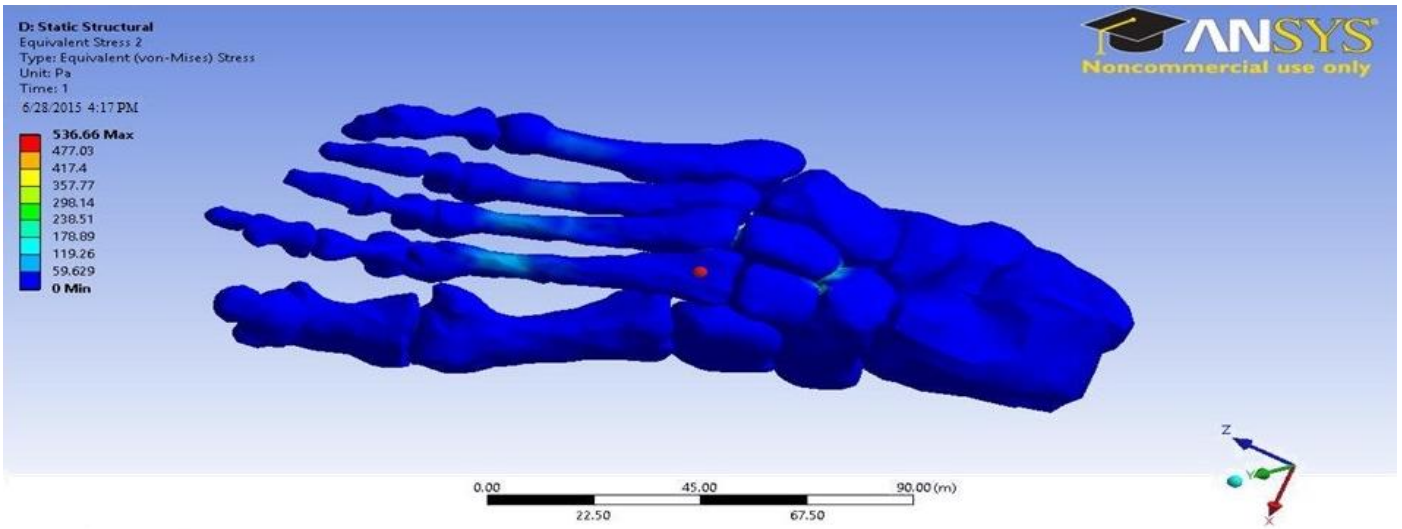


**Fig. 5.14** *Screenshot of Von-Mises stress of foot model by applying 700Nat an angle $120^0$*

By applying 800N at angle of $120^0$ the maximum Von-Mises stress was found to be 613.3 Pa and the minimum Von-Mises stress was 0 as shown in Fig.5.15. In comparison to the above two figures the maximum magnitude of stress in this case is largest.

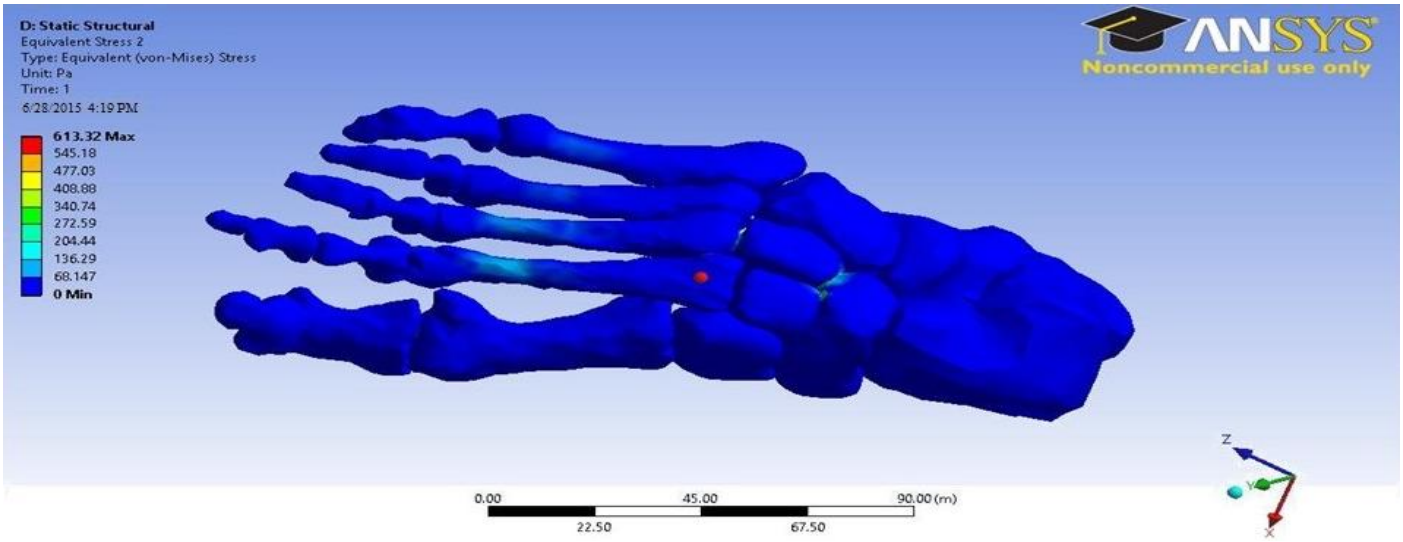


**Fig. 5.15** *Screenshot of Von-Mises stress of foot model by applying 800N at an angle $120^0$*

By applying 600N at angle of $45^0$ the maximum Von-Mises stress was found to be 412.98 Pa as shown and the minimum Von-Mises stress was 0 in Fig. 5.16.

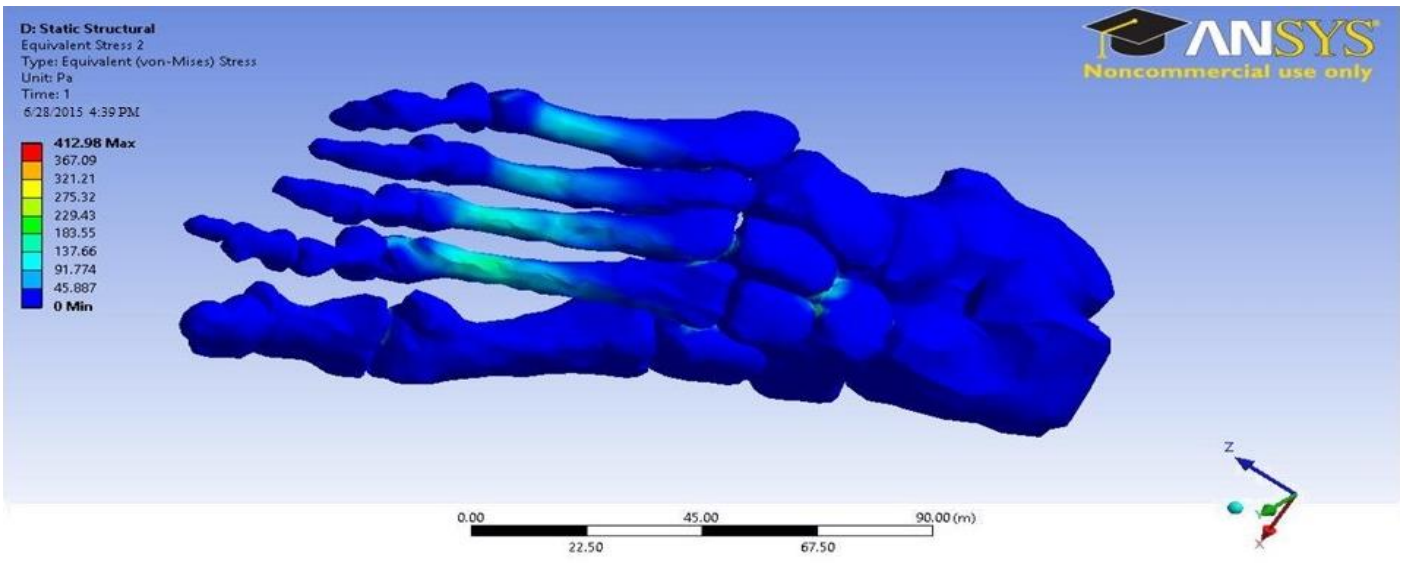


**Fig. 5.16** *Screenshot of Von-Mises stress of foot model by applying 600N at an angle $45^0$*

By applying 700N at angle of $45^0$ the maximum Von-Mises stress was found to be 481.81 Pa and the minimum Von-Mises stress was 0 as shown in Fig.5.17.

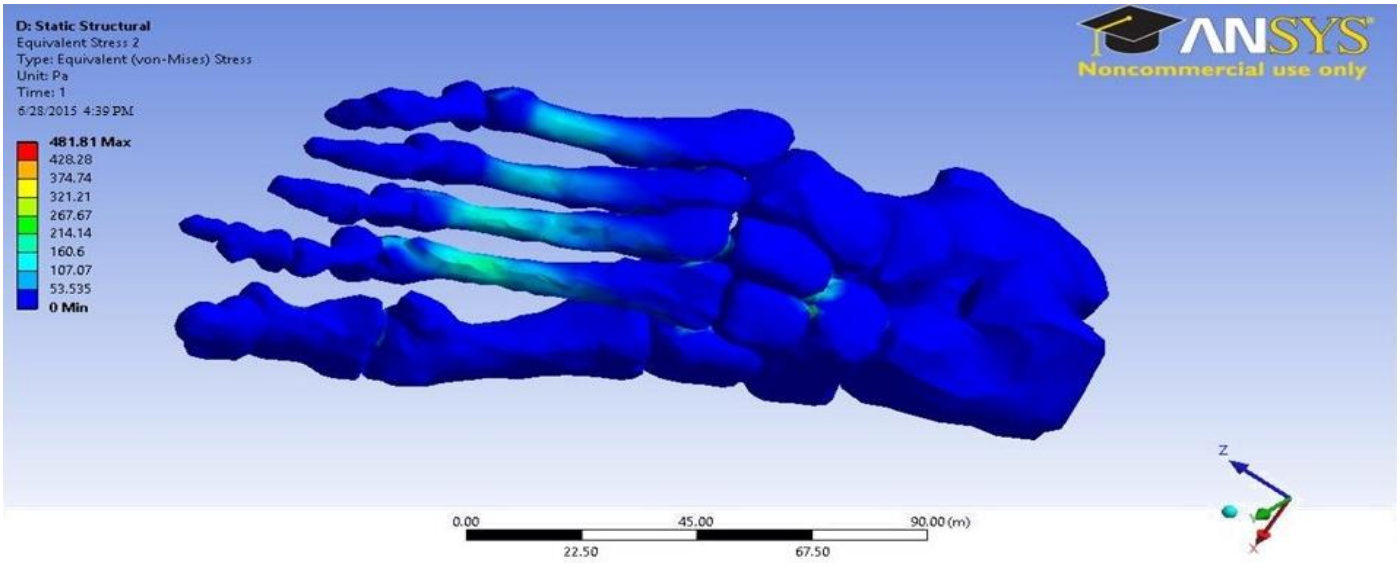


**Fig. 5.17** *Screenshot of Von-Mises stress of foot model by applying 700Nat an angle $45^0$*

By applying 800N at angle of $45^0$ the maximum Von-Mises stress was found to be 550.64 Pa and the minimum Von-Mises stress was 0 as shown in Fig.5.18.

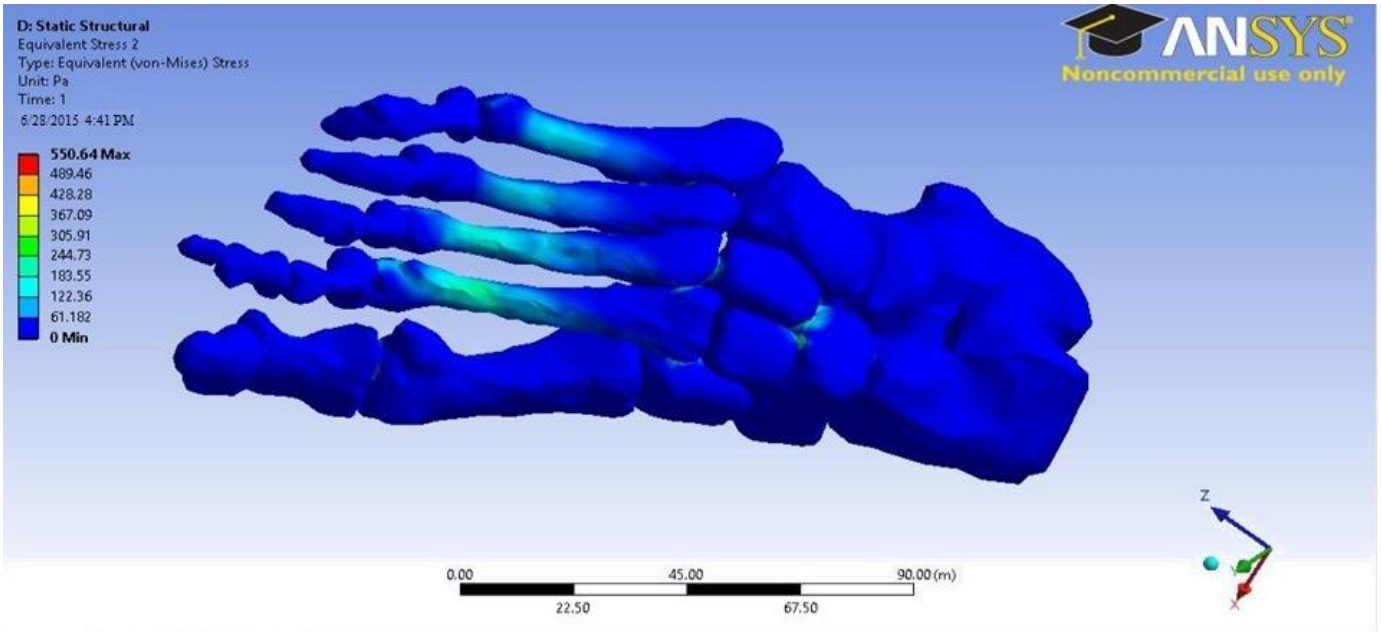


**Fig. 5.18** *Screenshot of Von-Mises stress of foot model by applying 800Nat an angle $45^0$*

| | Maximum Deformation(in m) | | | MaximumStress(in Pa) | | |
|---|---|---|---|---|---|---|
| Force Acting (in N) | $45^0$ | $120^0$ | $90^0$ | $45^0$ | $120^0$ | $90^0$ |
| 600 | .03965 | .025806 | .053553 | 550.64 | 459.99 | 978.66 |
| 700 | .04626 | .030107 | .062478 | 481.81 | 536.66 | 1141.8 |
| 800 | .05287 | .034408 | .066941 | 412.98 | 613.3 | 1304.9 |

**Table 5.1** *Results of the maximum deformation and stress obtained for different values of forces*

The data in the Table 5.1 shows that the variation of magnitude of deformation and stress of the bone follows the following trend:

For a constant angle of application of force, the maximum value of stress and deformation varies almost linearly, since $\sigma \propto F$ and $\Delta L \propto F$, where $\sigma$ is the stress, F is the force acting and $\Delta L$ is the change in length. And $F \propto MA$, M is the mass and A is the acceleration. So the stress distribution in the foot depends on the mass, geometry and structure of the foot model.

For a constant force, acting at different angles it is observed that magnitude of stress increases non-linearly with change in angle of application of force, whereas the trend of variation of maximum deformation value shows a drop in value at an angle of $120^0$ as compared to the values at $45^0$ and $90^0$.

Both the total deformation and stress is maximum when load on the foot has an angle of $90^0$ with the horizontal.

Total deformation was minimum while descending a slope at an angle of $120^0$, but stress was minimum during ascending or climbing a slope at an angle of $45^0$. The variations of total deformation and stress were indicated by different colours.

## 5.0 CONCLUSION

In this study, the total deformation and stress analysis was performed using ANSYS. The total deformation & stress was calculated by applying 3 different loads – 600N, 700N and 800N at 3 different angles - $45^0$, $90^0$ and $120^0$

The max. deformation value is obtained in the case of max. load i.e. 800 N, at an angle of $90^0$ , i.e., the case of mid foot strike. It was found that rear foot has more deformation than fore foot. Fore foot value for deformation is as low as 0 m and rear foot value is as large as 0.066941 m.

During descending a slope (at $45^0$) the foot has more deformation than ascending (at $120^0$), ranging from 0.03965 m, to 0.05287 m at an angle of $45^0$ and 0.053553 m to 0.066941 m at an angle of $120^0$. In all cases minimum deformation was found to be 0. From the above experiment, it is observed that the deformation increases gradually with increase in loads. For 600 N max. deformation is 0.53553 m, for 700 N it is 0.062478m and for 800 N it is 0.066941 m.

Similarly stress was calculated by applying various forces – 600 N, 700 N & 800 N. The corresponding stress values also increased with application of larger value of forces. For 600 N it was found to be 178.66 Pa, for 700 N it was 1141.8 Pa and for 800 N it was 1304.9 Pa.

The stress is found to be max. in metatarsals region and minimum in phalange region. Max. stress value is 1304.9 Pa for a higher force of 800 N in the metatarsal region and min. stress value for all cases was found to be 0.

From trend of values it can be deduced that the total deformation is minimum when force acts at an angle of $120^0$ on the ankle joint, and the deformation has maximum magnitude at an angle of $90^0$. Hence, it can safely deduce that the heel strike at an angle of $90^0$ should be avoided, as it might give rise to chronic problems such as planter fascitis, arthritis, heel spurs, stress fracture and bursitis. This has a great significance for sports persons (sports biomechanics). The heel strike angle should be kept less than $90^0$ and above or equal to $120^0$ for pain free performance.

# REFERENCES


[1] Attarian DE, McCrackin HJ, DeVito DP, McElhaney JH, Garrett WE Jr., Biomechanical characteristics of human ankle ligaments, *Foot Ankle*, pp 54-58, 1985.

[2] Ogilvie-Harris DJ, Reed SC, Hedman TP. Disruption of the ankle syndesmosis: biomechanical study of the ligamentous restraints, *Arthroscopy*, pp 558-560, 1994.

[3] Rasmussen O. Stability of the ankle joint. Analysis of the function and traumatology of the ankle ligaments, *Acta Orthop Scand Suppl*., pp 1-75, 1985.

[4] Harper MC., The lateral ligamentous support of the subtalar joint, *Foot Ankle*, pp 354-358, 1991.

[5] Kjaersgaard-Andersen P, Wethelund JO, Helmig P, Soballe K., Stabilizing effect of the tibiocalcaneal fascicle of the deltoid ligament on hindfoot joint movements: an experimental study, *Foot Ankle*, pp 30-35, 1989.

[6] Kjaersgaard-Andersen P, Wethelund JO, Helmig P, Soballe K., The stabilizing effect of the ligamentous structures in the sinus and canalis tarsi on movements in the hindfoot. An experimental study, *Am J Sports Med*., pp 512-516, 1988.

[7] Cass JR, Morrey BF, Katoh Y, Chao EY. Ankle instability: comparison of primary repair and delayed reconstruction after long-term follow-up study, *Clin Orthop Relat Res*., pp 110-117, 1985.

[8] Trouilloud P, Dia A, Grammont P, Gelle MC, Autissier JM., Variations in the calcaneo-fibular ligament (lig. calcaneofibulare). Application to the kinematics of the ankle, *Bull Assoc Anat (Nancy)*, pp 31-35, 1988.

[9] H.M. Frost, Bone modeling & skeletal modeling errors. Orthopedics Lectures, Springfield, Illinois, pp 45-49, 1973.

[10] F. Pauwels, Biomechanics of the Locomotor Apparatus, Springer-Verlag, New York, pp. 1-228, 1980.

[11] A. Dabrowska-Tkaczyk, M. Pawlikowski, "Influence of remodeling, stimulating factor selection on bone density distribution in pelvic bone model", Acta of Bioengineering and Biomechanics, pp. 119-126, 2006.

[12] Y. Shireesha, S. V. Ramana, and P.G. Rao, "Modeling and static analysis of femur bone by using different implant materials," IOSR Journal of Mechanical and Civil Engineering, pp. 82-91, 2013.

[13] J. Cheung, and M. Zhang, "A 3-Dimensional Finite Element Model of the Human Foot and Ankle for Insole Design", Academy of Physical Medicine and Rehabilitation, pp. 353-358, 2005.

[14] A. Gefen, "Stress Analysis of The Standing Foot Following Surgical Plantar Fascia Release", Journal of Biomechanics, pp. 629–637, 2002.

[15] M. Ozen, O. Sayman and H.Havitcioglu," Modeling And Stress Analyses of A Normal Foot-Ankle And A Prosthetic Foot-Ankle Complex", Acta of Bioengineering and Biomechanics, pp. 19-27, 2002.

[16] S.H. Kim, J.R. Cho, J.H. Choi, S.H. Ryu and W.B. Jeong, “Coupled Foot Shoe Ground Interaction Model to Assess Landing Impact Transfer Characteristics to Ground Condition”, Interaction and Multiscale Mechanics, pp. 75-90, 2012.

[17] R. Stallman, “Numerical Modeling of Human Foot”, Journal of Biomechanical Engineering, 2, pp. 29-55, 2013.

[18] Alberto Leardini, John J O’Connor and Sandro Giannini, “Biomechanics of the natural, arthritic, and replaced human ankle joint”, Journal of Foot and Ankle Research, pp. 3-14, 2014.

[19] Freitas F. A. S., Salviano. R. F., Rocha. D. N., Pinotti. D. Author, “Creation of a biomechanical model of the foot and ankle joint complex” , Blucher Mechanical Engineering Proceedings , pp. 67-84, 2014.

[20] A. Selk Ghafari, A. Meghdari, G.R. Vossoughi, “Contribution of the Muscles at the Ankle Joint during Daily Activities”, Center of Excellence in Design, Robotics and Automation (CEDRA), pp. 121-132, 2009.

[21] Carol A Oatis, “Biomechanics of the Foot and Ankle Under Static Conditions”, Journal Of American Physical Therapy Association, pp. 69-75, 1988.

[22] N.K. Singh, R. Braru, and S.K. Rai, “Development and Validation of Robust 3D Solid Model of Femur Using CT Data,” IRF International Conference, Goa, India, pp. 51-55, 2014.

[23] L. Peng, J. Bai, X. Zeng, and Y. Zhou, “Comparison of isotropic and orthotropic material property assignments on femoral finite element models under two loading conditions,” Medical Engineering Physics, pp. 227–233, 2007.

[24] C. Radu, and I.C. Rosca, “Modeling of the Hip Joint,” Annals of the Ordea university, Fascicle of Management and Technological Engineering, 745-750, 2007.

[25] M.J. Fagan, and A.J.C. Lee, “Material selection in the design of the femoral component of cemented total hip replacements,” Clinical Materials, pp. 151-167, 1986.

[26] E.Y. Chao, and K.N. An, “Biomechanical analysis of external fixation devices for

the treatment of open bone fractures in finite element,” in Biomechanics, R.H. Gallagher, B.R. Simon, P.C. Johnson, and J.F. Gross (eds.), John Wiley & Sons, New York, pp 124-147, 1982.

[27] N.S. Gokhale, S.S. Deshpande, S.V. Bedekar, and A.N. Thite, Practical Finite Element Analysis, Finite to Infinite, (1st Edition), Pune, Maharashtra, India, pp 47-244, 2008.

[28] http://www.learnengineering.org/2012/12/what-is-von-mises-stress.html

[29] http://aboutjoints.com/physicianinfo/topics/anatomyhip/biomechanicship.html

[30] http://www.sv.vt.edu/classes/MSE2094_NoteBook/97ClassProj/num/widas/history.html

[31] http://www.brighthubengineering.com/cad-autocad-reviews-tips/66732-what-are-the-steps-required-to-perform-a-finite-element-analysis/

[32] Basic Anatomical Terms and Definitions,www.footdoc.ca/ www.FootDoc.ca/ Website%20Definitions%20%28Basic%20Terms%29, 2014.

[33] Biomechanics of running, www.pt.ntu.edu.tw/hmchai/BM03/BMsports/Run, 2014.